
VISUOSPATIAL NAVIGATION FROM THE BOTTOM-UP: WITHOUT VESTIBULAR INTEGRATION, DISTANCE PREDICTION, OR MAPS

A PREPRINT

Patrick Govoni*¹ and Pawel Romanczuk^{1,2,3}

¹Institute for Theoretical Biology, Department of Biology, Humboldt Universität zu Berlin, Berlin, Germany

²Science of Intelligence, Research Cluster of Excellence, Berlin, Germany

³Bernstein Center for Computational Neuroscience, Berlin, Germany

December 5, 2025

ABSTRACT

Navigation is believed to be controlled by at least two partially dissociable systems in the brain. The cognitive map informs an organism of its location and bearing, updated by integrating vestibular self-motion or predicting distances to landmarks. Route-based navigation, on the other hand, directly evaluate sequential movement decisions from immediate percepts. Here we demonstrate the sufficiency of visual route-based decision-making in a classic open field navigation task often assumed to require a cognitive map. Three distinct strategies emerge to robustly navigate to a hidden goal, each conferring contextual tradeoffs analyzed at both neural and behavioral scales, as well as qualitatively aligning with behavior observed across the biological spectrum. We propose reframing navigation from the bottom-up, through an egocentric episodic perspective without assuming online access to computationally expensive top-down representations, to better explain behavior under energetic or attentional constraints.

Keywords · spatial navigation · visual perception · embodied cognition · sensorimotor learning · information processing

1 Introduction

Navigation involves correlating perceivable spatial features with expected goal location, whether it be food, shelter, or other area of interest, requiring the environment to be sensed and processed before effective movement. Cognitive maps, widely accepted as the ultimate way many organisms represent space, describe a system of hippocampal cells

*Corresponding Author E-mail: pgovoni21@gmail.com (PG)

tuned to distinct spatial elements collectively composing a Euclidean graph upon which direct pathways and novel shortcuts can be calculated via simple vector transformation [1, 2]. Although maps can be used for useful top-down planning, particularly regarding shortcuts, focus on this subset of navigational possibility has left its alternatives relatively understudied. Route-based navigation, on the other hand, concatenates sequences of egocentric movement decisions based on local observations, which can offer greater efficiency in complex environments [3, 4], or afford low demand reliability allowing energy to be directed to more critical or less predictable tasks [5]. Following familiar routes may rely on the bottom-up application of episodic memory [6, 7, 8, 9, 10, 4], a second key hippocampal function, while weaving together a network of routes enable construction of a non-Euclidean topology via state transitions [11, 12].

Map-based navigation algorithms often require online distance prediction [13, 14, 15], or otherwise vestibular integration [16, 17], in order to function. However, key visual dimensions were found to be functionally irrelevant for the two algorithms among those listed that performed ablation studies [16, 13], suggesting that vision provides a redundant information stream.

In contrast, many animals have been shown to principally rely on visual cues for reliable navigation. Gerbils and hamsters tend to use configurations of visible landmarks when well-lit, conspicuous, and reliable, otherwise resorting to their sense of self-motion [18, 19]. Similarly, the primate tendency to fixate our eyes rather than heads during self-motion may prioritize visual conflict detection over vestibular integration [20, 21], which would explain stronger hippocampal cell correlations to head orientation and visual perspective than to spatial position [22, 23, 24, 25, 26]. Even rats, with normally strong positional hippocampal correlations, lose spatial selectivity in virtual reality despite maintaining directionality [27, 28] and flexible navigation [10]. That is, restricting the vestibular sense forces a sequential route-based strategy grounded in vision.

Although visual distance calculation may be highly useful in specific contexts, e.g. cliff avoidance, prey capture, or jumping gaps [29], whether in the natural environment or in designed experimental paradigms, this perceptual dimension may not be as universal as assumed, or as accessible without considering its cost. Eliminating depth does not significantly affect visual orientation capability in hamsters [30]. Rats prioritize overhead binocular fusion over constant frontal depth perception, as the latter is not as critical for predator avoidance [31]. Additionally, complex 3D habitats may be required to justify its development [32].

On our way to work or the market, routes we know quite well, to what extent do we continually update distances to landmarks, or count our turns, rather than rely on relative positions of cues in our visual field? That allocentric map-based abilities both take longer to acquire and subside faster than egocentric navigation over the span of a lifetime suggests the preeminence of route-based decision-making in the context of constrained cognitive capacity [33, 34]. Rather than assuming unabated access to high dimensional representations and abilities, perhaps a simpler feedforward framework can explain a subset of navigational behaviors across the biological spectrum, which, given nature’s propensity to minimize energy, may be favored if performance is adequately robust.

In pursuit of this hypothesis, minimal visual perception-action loops of embodied agents, without predictive or integrative feedback, are trained with fixed environment, perceptual, cognitive, and action constraints to solve a classic spatial navigation task. Although the Morris Water Maze with random initialization is often described as testing map- or place-based navigation strategy involving vector calculation with respect to the hidden goal [35, 36, 37, 4], we intend to demonstrate how this task may be simply solved by egocentric visual observations and sequential routes. Furthermore, by minimizing assumptions specific to certain organisms, our conceptual approach seeks to maximize generalizability to discover fundamental properties of visual route-based navigation.

2 Results

Model design

The environment is designed to be minimally complex: a square grid with four distinct walls and a hidden circular foraging patch or goal. Using boundary walls restrains ability to estimate distance, forcing reliance on relative angles to grid corners as salient landmarks. Agents are initialized in random locations and orientations for each simulation. As intermediate temporal representations are purposefully left out in our study, they must instead rely on immediate visuospatial calculations to robustly reach the patch.

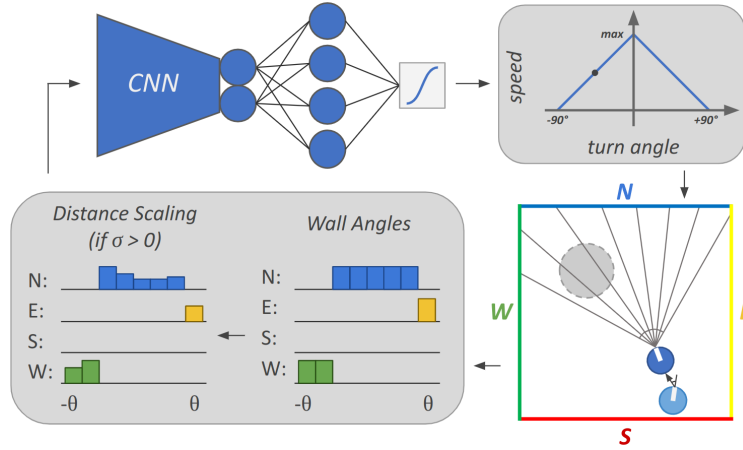


Figure 1: **Agent perception-action loop flow.** Clockwise from bottom left: visual encoding, information processing, action conversion, environment update. Visual encoding consists of identifying walls corresponding to retinal angles of a raycast (v number rays between $-\theta$ & θ field of view limits) for minimal angle-only vision, then adding distance information according to scaling factor σ . Visual information passes through convolutional neural network, perceptron, linear output layer, and hyperbolic tangent transformations to directly represent turning angle as well as speed via a linear function, which updates agent position and orientation for the next timestep (single update shown in environment and black point on linear function).

Inspired by [38], we simulated visual input as a raycast matrix, one-hot encoded per ray, extending from the agent to the boundary walls (Fig 1). Minimal vision provides information of identity and relative retinal angle of perceived walls, which we refer to as angle-based vision. For more complex vision, distance to the identified wall is logarithmically scaled into the encoding according to the Weber-Fechner law. In an unknown environment, accurate distance estimation requires higher order computation, e.g. stereopsis afforded by binocular fusion, static cues, dynamic temporal

inference, or memory. Angle-based vision, lacking distance information, represents minimal environmental information, constrained either from an estimation reliability or a cognitive load, attentional-based perspective. Vision with distance information, scaled in at increasing signal variance ranges, characterizes increasing perceptual ability or cognitive bandwidth, which may include predictive or integrative inferential capacities.

The information processing flow of an agent consists of three modules: a convolutional network (CNN), a single-layer perceptron, and a linear output layer. A CNN is chosen mainly for its image processing ability, though in part to its conceptual similarity and quantified correlation to the visual cortex [39]. A simple single layer feedforward downstream network was found to confer sufficient performance, whereas more complex architectures were found to provide minor additional benefit (S1 Fig). Finally, a single network output represents a ratio between turning angle and speed, a minimal action space constraint describing the need to slow down in order to turn. Note, this network is intended to be only phenomenologically related to sensorimotor information flow, rather than for specific biological detail.

The network is optimized via an evolutionary strategies (ES) algorithm. ES uses population-based black-box optimization without explicit gradient calculation, unlike reinforcement learning (RL) which optimizes a single agent by using backpropagation on a continuous differentiable objective function [40, 41]. Though both being mechanisms for optimization through perception-action-based interaction in the environment, they both result in the construction of useful learned representations [42, 43, 44].

Fitness, or performance, was measured as the time taken to reach the patch plus the remaining distance if the patch was not reached by the end of the simulation. The first term is the primary driver for judging how well the agent navigates and the second guides initial learning behavior. The relative weighting of each was varied in initial experiments but found to not make a significant difference.

Training

Training the networks to this navigation task revealed the sufficiency of route-based navigation in an open field (S1 Fig). Although only visual angle input is needed to adequately learn the task, performance and speed of convergence improves relative to the salience of an added distance signal. At maximal distance input ($\sigma = 1$), performance approaches the theoretical lower bound of perfect trajectories straight to the patch. Attenuating its signal gradually reduces utility of the distance information, describing a titration between angle-based and distance-based perceptual encodings. At $\sigma = 0.2$ signal variation is too subtle for the network to effectively use the information, slowing down learning rate and hindering performance, while at $\sigma = 0.1$ the signal is not evidently used at all.

On the behavioral side, a convergence into distinct classes was observed in the navigation trajectory space (Fig 2 top row, movies S1-S3). Two separate angle-only navigational strategies emerged despite identical constraints, best described by the terms "indirect sequential" and "biased diffusive". Adding distance scaling to the visual input resulted in a third class called "direct pathing". Hybrid strategies exist, indicating a continuum among clusters (S8 Fig), where exact boundaries depend on classification criteria details, discussed in Materials and methods.

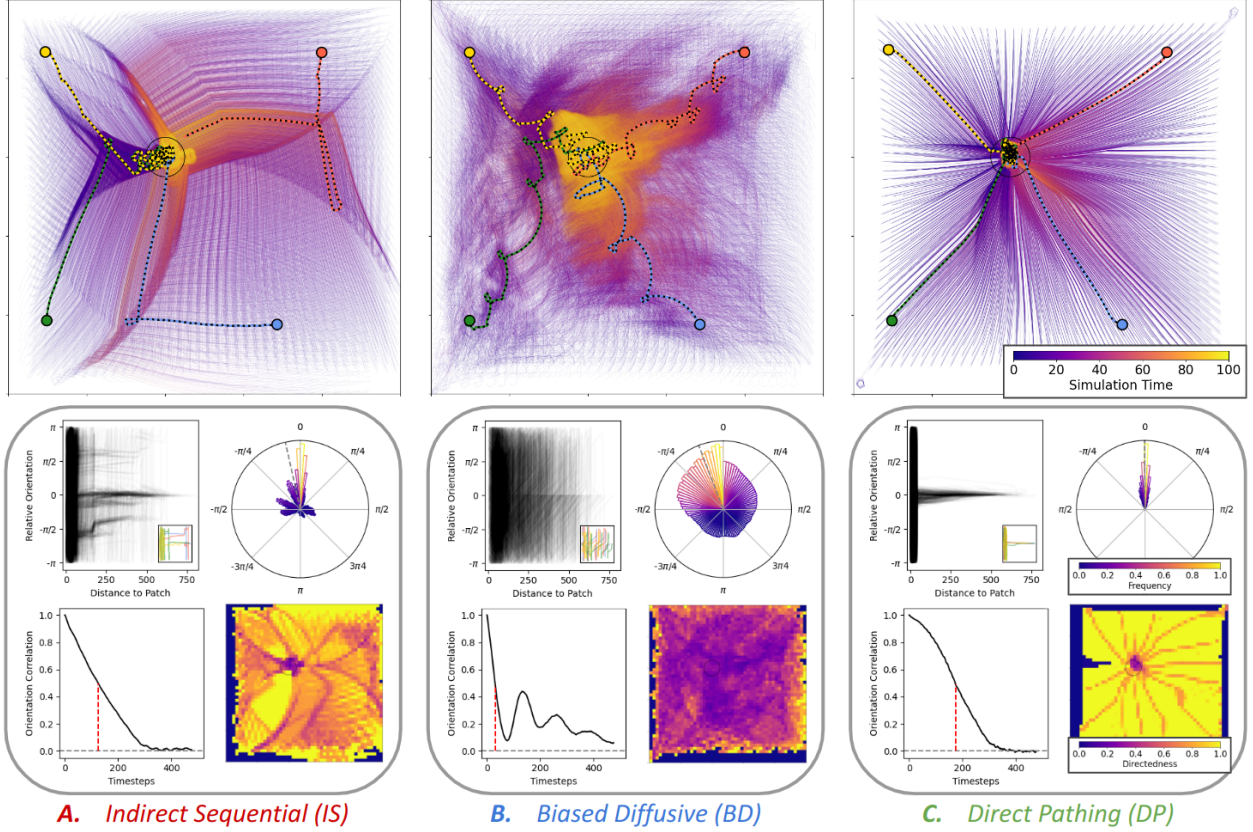


Figure 2: Three navigational classes, movement behavior & correlations. *Top row:* global movement behavior of three individual evolutionary runs or agents, with angle-based vision for A/B and with added distance scaling for C ($\sigma = 1$), each with an 8 ray visual resolution ($v = 8$). Solid lines: single agent trajectories from unique initial positions and orientations, temporally colored, density and darkness reflect common routes. Dotted lines: 4 example individual trajectories. Black circle: patch location. *Bottom row:* movement correlations. Top left: spatial heading profile with respect to initial heading and distance from patch center, inset shows same 4 example trajectories in above plots. Top right: polar histogram of relative orientation for timesteps when agent is over 100 grid units away from patch center, with frequency proportional to area and color of bin. Bottom left: temporal persistence of initial heading angle, marked by decorrelation time (50% threshold, red dashed line), sinusoidal shape reflecting correlated oscillations. Bottom right: directedness heatmap, an information theoretic measure calculated for each spatial bin in the environment. See S2 and S3 Figs for other individuals.

Angle-only navigation: behavior & mechanisms

The indirect sequential algorithm or class describes agents that learn to travel indirect trajectories to the patch, composed of a sequence of straight segments (Fig 2a). Elliptical arcs sweeping across the arena define transition points, scaffolding the route, which the agent uses to shift direction through a single sharp turn. Despite lacking distance perception, the agents learn to use visuospatial invariances afforded by the environmental structure in order to reach the patch. However which invariances to use and how to compose them into an effective strategy varies between runs (S2 Fig).

The route-determining elliptical manifolds are governed by a variety of environmental, perceptual, and movement constraints, coordinated to the patch location (S4 and S5 Figs, see Materials and methods). Mechanistically, the agent learns to tie major turn decisions to specific views with respect to two adjacent corners. As one of these views is rotated about the central axis of the respective wall, its decision threshold takes an elliptical form (S5 Fig, 1b). While these

manifolds cannot be easily seen by examining static neural activity normalized across location and orientation (Fig 3A), the ellipses are clearly evident when using goal-directed temporal data (Fig 3D). The goal location does not appear to spatially correlate with uniform grid data yet strongly overlaps with the visible manifolds in trajectory data (Fig 3A & D, left). However, directional components are not evident when deriving neural tuning curves for the former while strong 90 degree components arise in the latter (Fig 3A & D, right).

The movement profiles of the indirect sequential agents stand in contrast to the second class of algorithms, which can be distinguished by looping trajectories (Fig 2b). While overall progress is biased directly toward the patch, these agents regularly spin or turn, sensing and acting upon a wider set of observations. The trajectory maps render clouds of agent trajectories with little apparent correlation among each other, revealing no distinct manifolds or sequences, instead the process is diffusive.

Curving trajectories dynamically sample the entire range of orientations, obscuring movement patterns. Though its neural representation (Fig 3B) and vector field of action output (S6 Fig) show how learned gradients, scaffolded by the same elliptical manifolds, drive overall movement toward the patch, a mechanism that does not explain indirect sequential movement whose straight paths rely on a limited subsample of potential orientations. Goal location does correlate with averaged grid data for these agents, while the trajectory data seems less useful to describe mechanism. From a perturbative point of view, adding noise to the visual angle disrupts reliable indirect sequential navigation, while the biased diffusive agents remain robust (S7 Fig). Taken together, the agents traverse perception-action attractors approximately centered on the patch, structured via the same invariances perceived by the indirect sequential agents, yet their movement pattern differentiates how they are used.

Angle-only navigation: classification metrics

While the behavioral bifurcation between the two angle-based navigation strategies is qualitatively apparent, robust separability calls for quantified measures. General movement behavior can be compared by relating orientation to initial heading as an agent approaches the patch (Fig 2a/b, bottom row), demonstrating the tendency for straight, sparse or spinning, disperse profiles. However, though these plots provide useful intuition, extracting robust separation between the two classes for the entire range of agents has proven to be difficult, as can be seen in the extended figure (S3a/b Fig, bottom row, top plots).

Instead of tracking relative orientation in space, its temporal counterpart provides a cleaner split (Fig 2 bottom row, bottom left). Although other differences can be observed, the time needed for half of the agents to decorrelate from their initial heading consistently differentiates the two agent types. Biased diffusive agents quickly turn away, whereas indirect sequential agents follow their initial heading longer, until reaching an elliptical manifold.

Another way to track spatial correlation is via directedness, described as the orientational predictability of an agent at a given point in space. Average directedness is evidently lower for the biased diffusive agents (Fig 2 bottom row, bottom right). The measure quantifies observations made for the top correlation plots of Fig 2: indirect sequential agents

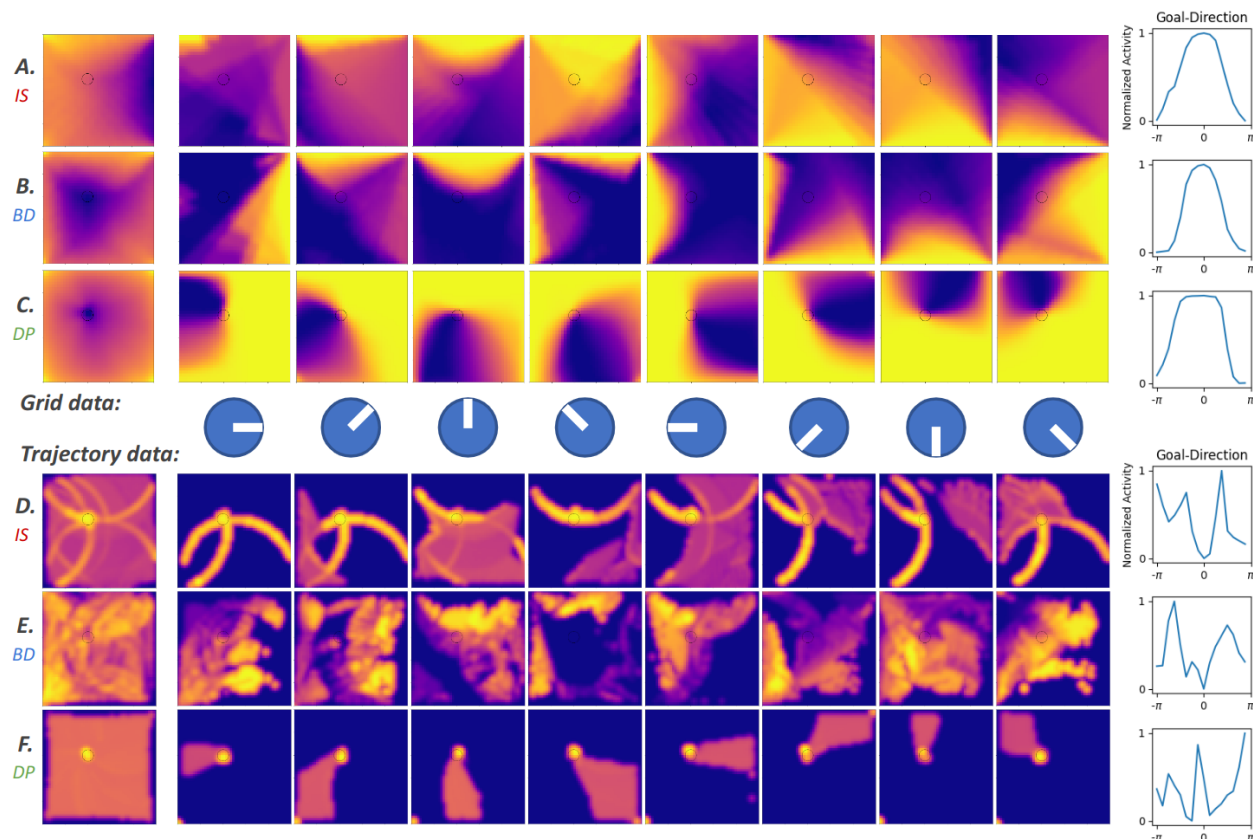


Figure 3: **Distinct approaches to represent neural data.** *Top:* neural activity data gathered with uniform spatial and orientational occupancy. *Bottom:* agents initialized as above, data gathered over 500 timesteps and binned in an equivalent manner. Left: spatial selectivity regardless of orientation, normalized from zero to maximum activation. Middle eight: spatial selectivity with respect to orientation, illustrated by agent directions. Right: neural tuning curves with respect to egocentric angle from the patch. A-C & D-F relate to the three agents and navigational classes of Fig 2: indirect sequential (IS), biased diffusive (BD), and direct pathing (DP).

tend to stick to few directions, while biased diffusive agents are more directionally indiscriminate. Yet for the former, directedness is locally low near elliptical manifolds and the patch, reflecting the wider range of potential directions at defined decision points, whereas there are no consistent spatial structures seen for the latter.

Angle-only navigation: separation & evolvability

Two clusters emerge in the phase space of decorrelation time and directedness, reflecting the qualitative separation observed above (Fig 4a, S9 top left). How such clustering arises can be seen by plotting average fitness values for each agent or run (S9 Fig, top right). Runs close to cluster centers tend toward the greatest fitness, while those farther tend to drop. Such gradients suggest the two clusters are attractors in a fitness landscape, where optimization pulls toward the centers.

Nonlinear dimensionality reduction techniques can find the gradient between the two navigational classes (S10 Fig) directly via the set of all possible visual observations and actions in the environment, however with lower explainability than using the two correlation metrics.

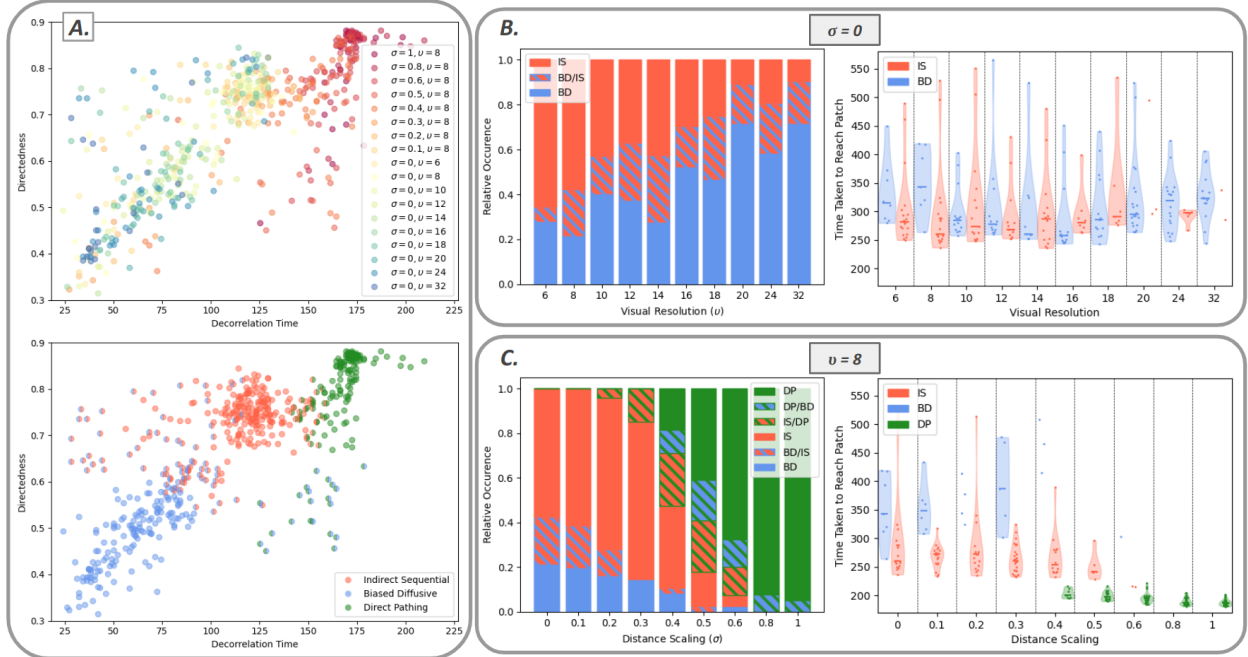


Figure 4: Classification & relative evolvability and fitnesses. A: Navigational algorithmic classes, separated by decorrelation time and directedness, top: colors correspond to distance scaling factor (σ) and visual resolution (v), bottom: colors correspond to algorithmic classes (IS: indirect sequential, BD: biased diffusion, DP: direct pathing), including hybrids as combined half-circles. B: Angle-based strategy bifurcation, left: relative rates of either angle-based classes evolving under different visual resolutions, right: relative fitnesses, revealing optima at $v = 8$ for IS and $v = 16$ for BD. C: Distance-based phase transition, similar plots as in B, varying distance scaling factors and $v = 8$. Scatter plots on right include violins for sample size greater than 5.

Given the asymmetric effect of noise to visual angle, it was expected that visual resolution would be critical in regulating preferential evolvability between the two classes. Indeed it is (Fig 4b): lower visual resolution favors learning an indirect sequential strategy, while higher favors biased diffusive. Whereas the indirect sequential mechanism involves distinguishing only few major transitions, biased diffusive perception needs to construct an accurate gradient with respect to the entire range of potential visual observations, locations, and orientations. Therefore, visual resolution, a parameter dictating the degree of environmental complexity able to be perceived, affects relative occurrence between strategies accordingly.

Relative fitness with respect to visual resolution shows a similar pattern (Fig 4b). Each navigational strategy confers similar optimal global performance, explaining why the behavioral bifurcation exists in this parameter space. However, visual resolution needed for the biased diffusive agent to meet this level is twice that of the indirect sequential, thus requiring twice the number of convolutional operations per timestep, as well as twice the complexity in the visuospatial affordance space (S5 Fig, 4th row).

Navigation with distance

Adding distance information to the visual input gives rise to a third class of algorithms that can travel directly to the patch (Fig 2c). Each agent differs in the degree and arrangement of how common routes collapse as they approach the

patch, though variation is slim compared with the two angle-based classes. The uniform directness of their routes is apparent in their relative heading profiles, long decorrelation times, and high directedness throughout the environment, with the exception of the patch area. Appropriately, their neural representations appear to outline clear directional trajectories to the patch position (Fig 3C/F) with oriented activations cleanly situated between environment boundaries and the patch. The goal position is outlined using either dataset, with strong orientational alignment when using grid data, appearing to represent a goal-direction cell [45] as well as behaviorally affording goal vectors regardless of initialization (Fig 3F, middle).

Distance-based navigation establishes a third cluster center in the correlation space, (Fig 4a). due to the lack of behavioral variability possible, whereas many different movement patterns can be classified under either angle-based class. As the distance signal is attenuated, relative occurrence of direct pathing agents decreases until the other two classes fully occupy the resulting space (Fig 4c left). Given that a sizable fitness difference between distance-based and angle-based strategies remains even with attenuated signal (Fig 4c right), the abrupt disappearance of direct pathing behavior suggests the networks are no longer able to effectively use the input.

3 Discussion

We trained a simple yet expressive artificial neural network to navigate toward a hidden patch in a robust and efficient manner (Fig 1, S1). By placing heavy constraints on perception, cognition, movement, and the environment, that is, monocular 1D visual perception, no predictive framework or within-trial memory, a single decision variable governing movement kinematics (turning & speed), and a four wall or landmark environment, we demonstrate the sufficiency of an egocentric, feedforward, route-based framework to solve the Morris Water Maze.

Three distinct classes of algorithms emerged in order to accomplish this, each with a set of distinguishable features (Fig 2, 3). The first class of agents navigate by composing a sequence of straight segments, indirectly oriented with respect to the patch, with major turns defined by elliptical-shaped manifolds, i.e. view-specific invariances stemming from perception of two adjacent corners. The second class instead learns to spin or diffuse toward the patch, driven by smoother global gradients constructed from the same elliptical invariances. And the third uses distance perception, a phenomenological implementation of advanced perceptual ability, to calculate near-ideal paths to the patch. Described via behavioral characteristics, these classes are termed indirect sequential, biased diffusive, and direct pathing, respectively.

The classes can be separated by two correlation metrics: decorrelation time and directedness (Fig 2), indicating temporal persistence in heading and directional potential in space. Biased diffusive has low measures for both, indirect sequential has medium, and direct pathing has high. The three classes tend to cluster into distinct bins in this 2D phase space, suggesting fitness-based attractors for movement correlation parameters.

Angle-based algorithms (indirect sequential and biased diffusive) confer comparable performance though prefer different visual resolutions (Fig 4). Indirect sequential agents evolve more readily and perform better with lower visual resolution

and biased diffusive with higher. While only requiring low quality visual signal and sparse orientational profiles, the indirect sequential agents are highly susceptible to visual angle noise throwing them off-course, whereas such noise does not affect the dynamic, disperse process of biased diffusive agents. Distance-based, direct pathing agents perform better than either angle-based class, resulting in an abrupt phase transition as the distance input becomes computationally usable, although requiring another dimension to their perception.

Vision vs. vectors

Our understanding of route-based strategies lags behind that of cognitive maps, in part due to historical preference for the latter [46, 47, 11, 8, 9]. Predispositions toward maps persist via experimental paradigms that reinforce the primacy of Euclidean graphs, despite partial dissociability and parallel use of the two strategies, and even despite results demonstrating similar rates of navigational success with either strategy [48, 49, 50, 7]. Whereas calculating shortcuts or direct trajectories are certainly optimal in certain scenarios, overemphasis on cognitive maps denies both value and understanding of route-based systems.

Given that map-based knowledge demands construction of a recurrent internal world model to predict and integrate external dynamics, complexity required presumably far surpasses systems that directly respond to visual input. Assuming a given organism would seek to minimize computational complexity while maintaining successful performance, external factors such as environmental context play a critical role in determining which system preferentially develops. For example, path integration may be ideal for desert ants which require precision to quickly return home after foraging in midday heat [51], though may cause problems in unpredictable areas with potentially dangerous shortcuts. Route-based representations, in contrast, have been suggested to favor dense environments with many navigational constraints or without ambiguous landmarks such as jungles or mazes [52, 3, 53]. What has not been evidently studied is their sufficiency in open arenas, an environment suggested to favor cognitive maps [14]. Our results present non-intuitive evidence: navigational strategies based on visual routes can perform well in open arenas.

The reinforcement learning community represents the navigational dipole somewhat differently. Model-based learning entails planning upon a predictive, goal-directed framework by constructing a model of external dynamics, while model-free works directly on cached action-value pairs [54, 55]. Described in this way, model-based learning appears to reflect map-based strategies and model-free to response sequences, coordinated through associative memory, [52, 42], though the two perspectives may not fully align [56, 57, 44]. Despite discrepancies, balanced theoretical and experimental effort toward both model-based and model-free reveals contextual advantages for each. Model-based learning tends to be more efficient in learning, as well as flexible and theoretically effective in control, yet require significantly higher capacity to handle complex external dynamics, which in turn may lead to overfitting [58, 59]. In contrast, model-free learning is computationally cheap and effective at scale.

Neural connections

The hippocampus and striatum are typically contrasted with respect to the Morris Water Maze, where the former is responsible for map-based, allocentric strategy with a focus on environment boundaries and distal (extra-maze) landmarks, and the latter for response-based, egocentric strategy using proximal (intra-maze) landmarks [60, 7, 4]. One possibility not examined in this dual-solution focus is the construction of egocentric routes based on boundaries and distal landmarks [61]. Accounting for this third option, i.e. equating routes as sequences of decisions, may help unite seemingly disparate functions of the hippocampus: spatial navigation and episodic memory [7, 62, 8, 9, 10, 4]. Rodents with hippocampal lesions are confined to beaconing, thigmotaxis, and scanning behavior [63, 64, 65, 4], while this can be understood as inflexible striatal navigation, it does not relate to the robust, initialization-invariant routes seen in our trained agents. The neural-semantic dipole between hippocampal-maps and striatal-responses does not leave room to allow for flexible route-based navigation, which presumably uses hippocampal episodic sequences to navigate via both egocentric responses and allocentric boundary or distal information, yet without demanding the ability to localize or plan on a map-like substrate.

The distributed nature of these systems generates degeneracies on multiple fronts in the solution space, allowing an organism to choose which pathway might suit the context. Outside the hippocampal-striatal dipole, several other cortical areas process navigational information, including: the retrosplenial cortex [66], occipital parietal cortex [67], and even visual cortex [68]. As described in the introduction, two recent models that allow for visual information, as well as vestibular [16] or distance [13], did not learn visual dependencies. While the former two information streams and learned representations are sufficient for the task, they are incomplete on their own [4, 69]. Reflected in neural architecture, two distinct sets of head direction cells are suggested to be updated via either self-motion or visual cues [70, 71], though see also evidence of integration [72]. Guidance and aiming tasks have been shown to prefer allocentric and egocentric action spaces, respectively, though both can be solved with the other regardless [44]. An important point not often discussed, let alone remedied, the Morris Water Maze does not adequately separate guidance from map navigation [4]: since landmarks are available from every point in the environment, triangulation via visual angles may be easier than self-localizing and computing vectors on a coordinate system [35, 36]. Degeneracy in the cognitive, sensory, action, and task spaces affords no easy answers. One way to inspect such systems is to focus on silencing or perturbing parts of these pathways [63, 27, 28, 64, 10, 44], and another, used here, is to explore a simple model constrained along one particular, under-studied pathway.

But does the agent learn a map? The agent learns to approximate a function that transforms egocentric observations into useful actions. Learned neural representations show significant directional modulation (Fig 3), aligning with a flight of papers on rodents in VR [27, 28, 10] and a modeling study examining task and action constraints [44]. Neural tuning corresponds with patch location, mirroring reports of representations with respect to goals [45, 73], as well as boundaries and landmarks [62, 74, 72]. The elliptical manifolds of the indirect sequential strategy trace view-specific correlations widely observed in primates and humans [22, 23, 24, 25, 26], which may be linked to egocentric cells

that conjunctively encode distance [9]. While we do not rule out the possibility of adapting these learned visuospatial functions to a map where the agent can plan trajectories, through the architectural constraints of our model, we have demonstrated that this externalization is not necessary. Similar to a minimal model by Bastien & Romanczuk proving vision alone can explain collective behavior without the need for higher level representations [38], and echoed by studies on sensorimotor contingencies and enactivist robotics [75, 76, 77], the main point of our model is to show that directly perceived routes provide sufficient navigation without requiring map-based inference.

Moreover, correlating average neural activity with the external environment may mislead. The averaging of neural activity of our evolved agents over space and time reveals activity patterns correlated with goal direction (Fig 3A/B, right). However, a corresponding goal signal is absent in time-resolved activation patterns governing actual movement decisions of our agents (Fig 3D/E, right). Thus, the general question emerges whether empirically observed, averaged activation patterns correlating with higher-order task features are indeed involved in decision processes in real-time, or whether they may emerge as a "by-product" of learning the task via low-level decision rules (e.g. indirect sequential) and a corresponding averaging procedure. Or to put it in other words: to what extent are map-based representations, extracted through averaged activity patterns, directly involved in the generation of behavior, rather than a necessary statistical consequence of a complex neuronal system learning a spatial task? A recent studies shows how neural activity describes internal action sequences rather than external variables [78], which may help explain why it is difficult for us to integrate between routes [79, 11]. Characterizing behavior provides a complementary perspective to mean field neural analysis [61], which may even be critical to understand direct perception-action behavior. While directional modulation may describe average neural correlation, clockwise curving trajectories may indicate a biased diffusive navigational strategy [10] or attractor-like alignment may indicate the use of visual manifolds [44].

Behavioral convergence

Rodent paths observed in the Morris Water Maze reflect movement characteristics from each of the three classes in the present study. While many learn how to take optimal direct paths, others travel in clearly wrong directions before abruptly turning toward the patch [80, 65, 81]. Although often termed "indirect search", this pattern parallels the indirect sequential navigational strategy. Other rodents instead walk toward the patch yet spin as they approach, attributed as "self-orienting" or even "nonsense movements" of "directed search" [82, 80, 65, 81], they mirror biased diffusive trajectories. Shifting perspective to view such behavior as essential components to egocentric navigational routes, as opposed to search behavior or errors relative to ideal trajectories, may yield novel hypotheses. Perhaps these rodents prioritize angular over distance information [30, 31, 32]. Balanced relative occurrence metrics and across-trial stability of the three strategies [82, 80] suggest each may confer contextual tradeoffs, where diversity has evolved to ensure robust population-level fitness in a variable environment.

The biased diffusive trajectories appear to mirror the helices of sperm cell chemotaxis [83, 84]. Sperm cells modulate swimming path curvature via temporally sampled chemical concentrations to bias motion up-gradient towards an egg. Despite clear differences in perception and movement capabilities, both learn a similar movement strategy to robustly

navigate to a hidden target. Though clearly the mechanisms differ, as sperms cannot see, the higher level phenomena seem to overlap, suggesting fundamental algorithmic properties for gradient navigation, which may be either directly sampled or indirectly constructed via angle-based vision.

Elliptical decision-making thresholds have been recently found to govern spatial bifurcations between choices or goal vectors [85, 86], in the same way ellipses spanning adjacent corners govern turn decisions for the indirect sequential agents. Fruit flies, desert locusts, and zebrafish have each been observed to move toward the average of two choices until reaching a critical threshold, spontaneously forcing a decision towards one or the other choice, even in sequence if more than two are available. While in the current study, perception-action loops learned to deterministically use elliptical thresholds to compose route segments, here they were used by a ring attractor model to stochastically choose between goals or sets of goals. Despite differing computational, algorithmic, and implementational level details, resulting behavior appears to have converged on a fundamental element: angle-based or view-specific turn decisions with respect to two spatially distinct entities, proposing a non-Euclidean spatial representation.

While there are speculative comparisons to make between our model and biology, there are limitations. The model is intended to be phenomenological, thus only general relations should be made. Although our convolutional neural network may reflect the visual cortex [39], its operations as well as the downstream layers are meant to ambiguously define sensorimotor perception-action information flow rather than specific brain regions or operations. Complexity has been reduced to a simple feedforward network, whereas the visual cortex and associated structures contain recurrent connections. Similarly, neural network optimization accumulates thousands of parallel perturbations and experiences each round, and thus is intended to reflect neither the speed nor mechanism of biological learning, nor does it reflect the search process preceding navigation. Only the behavior of a fully trained network is intended to be related to behavior of fully trained animals or humans.

Shifting perspectives

Rather than assuming the entire range of perceptual and cognitive capabilities of organisms when modeling behavior, probing minimal sufficient conditions for successful behavior under energetic-bound constraints offers unique insight into how organisms may behave outside the lab. Though many organisms may have the ability to construct predictive frameworks or integrate vestibular cues, a simpler feedforward system might do just fine, without the energy expenditure. That the resulting behavior and neural correlates track with phenomena covering rodents, insects, fish, and primates, provides evidence that such constraints may be widely applicable. These simple models do not assume navigation behavior to solely rely on one of the observed strategies, but rather suggest low dimensional visual techniques that can be used to save memory or complexity.

This is not intended to argue against the importance for cognitive maps, distance perception and prediction, or vestibular integration, nor to deny crossmodal interactions between map and route pathways, but rather encourage a plurality of perspectives moving forward. Given our historical bias toward top-down representation, as well as our physical

experience using maps or viewing rodents in a maze beneath us, we need to approach the egocentric, route-based perspective with a new lens. Route-based navigation can provide a fully separable navigational strategy with its own mechanisms and logic, demanding novel experimental methods for disentangling systems and characterizing mechanisms, proposing alternative navigational hypotheses to contend with assumptions of search or errors. Each system has characteristic advantages and disadvantages, with evolution and development shifting the balance toward a particular direction in a given environmental context. Only by understanding both can we more fully grasp the breadth of tools potentially available to a navigating organism.

4 Materials and methods

Visual encoding

Vision is simulated as a raycast originating from a single retina at the front edge of the agent, the orientation of both visual retina and agent are bound as a single state variable. Perceptual input is structured as a 1D array with each element one-hot encoded with respect to wall identity. Though a simplification from 2D vision, collapsing the vertical dimension has been previously found to retain sufficient directional information for visual navigation [87, 88].

Two key hyperparameters govern the raycasting process: field of vision (FOV) and resolution. FOV stretches the limits of the raycast with respect to the agent, and resolution determines the number of rays to cast within these limits. The FOV is set at 40% or 144 degrees to mirror the functional visual field for humans, as measured by reaction time to discrimination tasks [89], though the impact of FOV on navigation performance was also assessed (S1 Fig, 1st row). The visual resolution (v) is minimally initialized at 8 rays for much of the analysis and later varied to examine its effect on behavior (S1 Fig, 2nd row).

Weber-Fechner logarithmic scaling is applied for distance information, similar to how height is perceived by our eyes [90]. The scaling is calculated as follows:

$$y = -\frac{1}{k(\sigma)} \ln(x) + m(\sigma) \quad (1)$$

with x representing distance from the perceived environmental boundary, and k and m fixed according to the distance scaling factor σ , by relating minimum and maximum possible visual distances to a fractional visual encoding range. This difference in distance results in maximal encoding variance at $\sigma = 1$, and to 10% of the encoding space $\sigma = 0.1$.

Environment

The arena is defined at 1000 x 1000 units and the patch at 50 units. The patch to arena ratio correlates a 1-2 m diameter arena and 10-15 cm diameter platform often used for rodents in the Morris Water Maze [82, 80, 65, 81, 16]. An arbitrary timescale was chosen for our simulations, with a maximum agent speed at 2 units per timestep. This could be shifted to describe a lower or greater decision and action speed to reflect rodents, humans, or other organisms.

Environmental geometry provides the spatial reference needed for both orientation and location [91]. Although landmark and geometric encoding have been argued to be performed by separate modules [92, 93, 94, 60], in the present study the two are not differentiated.

Network architecture

The CNN used is a simplified version of the ConvNeXt v2 architecture [95, 96], a state-of-the-art design that outperforms earlier variations in the CNN design space and rivals the best vision transformers. While simpler designs exist, the ConvNeXt was chosen for its separable depthwise and pointwise convolutions, where separate parameters act on the orthogonal depth and channel axes, enabling greater expressibility for relatively low additional computational cost. A transformer was not chosen since they lack biological inductive biases, such as translation equivariance, and due to their novelty, lack the understanding and tools currently available for CNNs [97].

Beyond critical minimal values, depth and dimension of the CNN and perceptron did not noticeably affect performance (S1 Fig, 3rd/4th rows). Notably, two channel outputs for the CNN is insufficient for agents to reliably solve the task, possibly reflecting an intrinsic, minimal dimensionality to the navigation problem [98]. For more complex and recurrent architectures, as well as those with proprioceptive feedback, data at adequate sample size is forthcoming at the time of submittal and will be appended upon review. The activation function used for the CNN is a rectified linear unit. A sigmoid linear unit was found to net marginal performance increases, though slower simulation times.

The number of parameters is less than 300 for the models presented in the main text, significantly less than the tens of thousands needed for the predictive navigation network used in [13], and still less than the thousand needed for the non-visual linearized predictive networks in [15].

Agent movement

Network output is a single continuous value that directly represents turning angle for the next timestep, bounded by 90° left to 90° right via a hyperbolic tangent function. Speed is scaled by the output via a linear function, with zero representing maximum speed and both left and right limits for when the agent is stopped.

Collision with the foraging patch results in simulation termination when training, but no effect when testing. Collision with the boundary stops the agent from traveling out of the environment but allows rotation, it does not result in repulsive physical effects or a change in sensory input.

Optimization

The ES algorithm used is Policy Gradient Parameter Exploration (PGPE) using the ClipUp optimizer [99, 100], with parameters outlined in Table 1. Among various ES algorithms, PGPE was chosen for its balance between performance and speed, with greater performance than OpenAI-ES and greater speed than CMA-ES [101]. ES entails less complexity

than RL, as there is no need for differentiability, value approximation, or within-trial credit assignment [40, 41]. The main drawback of ES, sample inefficiency, is acceptable given its parallelizability.

Table 1: **Hyperparameters used for the ES algorithm**

Name	Value
Generations	1000
Episodes	20
Population Size	50
Standard Deviation, Initial	0.1
Standard Deviation, Learning Rate	0.1
Standard Deviation, Max Change	0.2
Mean, Learning Rate	0.2
ClipUp, Momentum	0.8
ClipUp, Max Speed	0.4

Training, validating, testing

Fitness performance during training was calculated as the time taken to reach the patch plus remaining distance if the agent has not reached the patch within simulation time limit (1000 timesteps). Alternative scalings were tried but found to not make a significant difference.

Validation was performed to more robustly test performance from a wider range of initializations than the episodes during a training generation. Twenty of the top performing generations were chosen, using the population parameter center for each, with 100 initializations for each. Remaining distance from the patch was not included for the validation data.

The agent was tested by simulating the top agent of an evolutionary run at different initializations across the grid, spaced every 25 units and oriented in 16 directions. Each initialization was run for 500 timesteps, regardless if the agent collides with the patch. The test data from this set of trajectories was used for Fig 2.

Elliptical manifold perception

How the elliptical manifolds, explicit for the indirect sequential agents (Fig 2a) and implicit for the biased diffusive agents (S6 Fig), can be examined directly via perturbations. Perceptual, environmental, and movement related parameters all affect the shape and location of the manifolds (S4 Fig).

Inferring the generative mechanism, given the ellipses emanate from two adjacent corners, the manifolds may be marked by two raycasts simultaneously intersecting both corner locations, representing a change in wall perception in both corners at once. A numerical search for these ideal locations shows that simultaneous dual corner detection reconstructs elliptical arcs, with orientation rotated about the center between the two corners, and both perturbed FOV and visual resolution shifting the arcs predictably (S5 Fig, 1st & 4th rows).

While perceptual and environmental parameters are fixed for a given training period, movement dynamics can shift manifold positioning as needed. Generated ideal elliptical arcs intersect with patch position at FOV of 40%, but not for 35 or 45. Though when trained with these FOVs, the agents learn to approximate ideal arcs useful for calculating patch position regardless (S5 Fig, 2nd row). By increasing turning speed before intersecting with a manifold, the agent expands its capacity to perceive a corner, thereby allowing the agent to effectively precede ideal arc location. Looking at turning speed for each agent, it is clear that the agents with FOV 35 or 35% increase incoming turning speed in order to shift the ellipse to a more useful position (S5 Fig, 3rd row). Thus, although various perceptual, action, and environmental parameters constrain elliptical manifold construction, the learning algorithm coordinates movement behavior such that generated ellipses facilitate navigational success.

Furthermore, mean field analysis can demonstrate how the two angle-based classes use the elliptical manifolds differently (S6 Fig). Indirect sequential agents (a) can sufficiently navigate without minima overlapping patch location since their algorithm relies on a sparse, stable subsample of orientations. Biased diffusive agents (b) navigate with respect to a disperse, dynamic sample of every orientation, thus their success depends on correlating mean field minima with patch location. Elliptical manifolds visibly structure attractors for both angle-based classes, and are not apparent with the smoother gradients of distance-based agents (c). Higher visual resolution angle-based individuals (bottom row, a/b) tend to exhibit increased elliptical manifold presence (south & east walls), possibly explaining why biased diffusive agents perform better at greater visual resolution.

Movement correlations

All movement correlations were transformations of the test trajectory data previously described. The first 25 timesteps, when the agent is orienting itself upon random initialization, are cut out when calculating movement statistics. Thus, the orientation at $t=25$ represents the initial route heading.

The spatial heading profiles of the top left correlation plots in Fig 2 were produced by plotting agent orientation relative to the initial route heading against the distance from the patch center. The polar histograms count the frequency of relative orientations, where the area under each bar is scaled to relative frequency.

The temporal correlation metric uses a function borrowed from a sperm chemotaxis paper [102], given the similarity between movement trajectory patterns:

$$C(t) = \langle \cos[\phi(t_0 + t) - \phi(t_0)] \rangle \quad (2)$$

with ϕ representing the orientation angle of the agent and t_0 defined at a delay of 25 timesteps from initiation. Decorrelation time is defined by the length of time needed for Ct to drop below half.

Directedness, the spatial correlation metric, is based on the range of directional possibilities available to the agent, mapped across space. We calculate the information entropy [103, 104] of the orientational frequency distributions for each spatial bin across the environment:

$$H(\Phi, b) = - \sum_{\phi \in \Phi} p(\phi) \log(p(\phi)) \quad (3)$$

with H being the directional entropy, Φ being the set of 16 orientations, and b the spatial bin. Bounding to the range of entropy values possible for Φ and inverting, we arrive at a measure of directedness:

$$D(H, \Phi, b) = \frac{H_{max}(\Phi) - H(\Phi, b)}{H_{max}(\Phi) - H_{min}(\Phi)} \quad (4)$$

Given the initial delay and that trajectories generally move toward the center of the environment, the edges of the environment contain lower data density, thus data 100 spatial units away from the boundaries were masked out of the calculation of directedness. Trajectory information near the patch is external to navigation behavior, thus data 100 units from the center of the patch were masked out as well. Final values used were the average directedness calculated for the remaining spatial bins.

Neural representation

The activation profiles of perceptron nodes were plotted with respect to spatial position in the environment and orientation, or head direction as head and body are not separable in our model. Datasets used for the grid plots (Fig 3A-C), same as for S6 Fig, consisted of node outputs for a static, uniform sample of agent locations and orientations. Datasets for the trajectory plots (Fig 3D-F) were the same as used for the movement correlations. Using either dataset, output activity was sorted via 50x50 spatial bins, averaged within each bin, smoothed with a Gaussian filter of standard deviation 1, and plotted from zero to maximum activation. The data was further sorted into 8 orientation bins and separately plotted. This procedure follows a recent paper that focused on constructed activation rate maps from neural networks trained to navigate [44]. Neural tuning curves were plotted by binning activation according to the angle between the agent and the goal, as in [45].

Classification procedure

Classifying navigational strategies entailed two phases: binning then qualifying. First, bins were constructed in the 2D phase space of decorrelation time and directedness. The boundaries were conservatively drawn so as to limit any potential mixing with hybrid strategies. All agents with decorrelation time below 90 and directedness below 0.6 were labeled as part of the biased diffusive class, those with decorrelation time between 105 and 140, with directedness above 0.65 were indirect sequential, and with decorrelation time above 155 and directedness above 0.65 were direct pathing. Remaining unlabeled runs in the hybrid zones were classified according to a subjective summation of trajectory maps

and all movement correlation plots, as a more quantitative method was deemed to yield marginal relative value. A small quantity of previously binned and labeled runs were relabeled as hybrids, despite the results of the two metrics. Relative occurrence plots visualized the same labeled data with respect to visual resolution and distance scaling information.

While the clusters are visually separable, unsupervised clustering algorithms learn to draw in a similar way (S9 Fig, bottom row). Although unsupervised clustering algorithms can designate boundaries, hybrid strategies between or far from cluster centers require qualitative context.

Bottom-up dimensionality reduction

To complement the classification procedure, nonlinear dimensionality reduction algorithms provide a bottom-up, however less explainable means to separate navigational strategy. The set of actions related to all possible visual observations throughout the environment fully describe agent behavior. Agents with differing visual resolutions have access to differing numbers of possible visual observations. Lower visual resolution allows a lower total number of views than higher. A basis was chosen with visual resolution 8 with 132 unique views. The corresponding mean positions and orientations standardized the set of visual observations for every agent. The absolute value was taken for the resulting 132 actions, as agents learned to prefer clockwise or counterclockwise turning, and this break in symmetry is irrelevant to the classification of navigational strategy.

The results of two popular nonlinear dimensionality reduction algorithms, t-SNE and UMAP, both demonstrate separation aligning with our classification (S10 Fig). The direct pathing class distinctly separates from the two angle-based classes, and the indirect sequential and biased diffusive stretch along a gradient in another cluster. The clear distinction separating distance-based and angle-based navigational strategies, intuitively aligns with expectations. The graded cluster of the two angle-based classes suggests a continuum rather than separation, which may perhaps be more apparent when measures other than decorrelation time and directional entropy are taken into account. Despite such possibility, both decorrelation time and directional entropy appear to align with the separation and gradient of the two dimensionality reduction procedures. Though the former more smoothly aligns, especially considering the DP/BD hybrid agents.

Prior to t-SNE or UMAP, the data was passed through PCA to identify the 50 most principal components, a practice cited to reduce noise and high dimensionality. In practice, it did not appear to give a significantly different result.

Gaussian mixtures were applied to the t-SNE and UMAP results, demonstrating that unsupervised classification draws boundaries in a similar way to our metric-based procedure (S10 Fig).

5 Acknowledgements

Ideas within this paper were inspired from discussions at CapoCaccia Cognitive Neuromorphic Workshops (CCNW) 2024, especially those with Gabriel Gattaux, Andrew Philippides, and Florian Engert. Discussions with Nereu

Montserrat Busquets, Clemence Bergerot, Yunus Sevinchan, Valerii Chirkov, and Valentin Lecheval, have proven to be invaluable in developing the concept and delivery of the paper.

P.G. acknowledges support by the Elsa-Neumann-Stipendium by the state of Berlin under Nachwuchsförderungsgesetz (NaFöG) - application number H75014. P.R. acknowledges funding by the Deutsche Forschungsgemeinschaft (DFG, German Research Foundation) under Germany’s Excellence Strategy – EXC 2002/1 “Science of Intelligence” – project number 390523135.

All code and data used for this paper is publically available at <https://github.com/pgovoni21/vis-nav-abm>.

References

- [1] Russell A Epstein, Eva Zita Patai, Joshua B Julian, and Hugo J Spiers. The cognitive map in humans: Spatial navigation and beyond. *Nature Neuroscience*, 20(11):1504–1513, November 2017.
- [2] Jacob L. S. Bellmund, Peter Gärdenfors, Edvard I. Moser, and Christian F. Doeller. Navigating cognition: Spatial codes for human thinking. *Science*, 362(6415):eaat6766, November 2018.
- [3] Michael Peer, Iva K. Brunec, Nora S. Newcombe, and Russell A. Epstein. Structuring Knowledge with Cognitive Maps and Cognitive Graphs. *Trends in Cognitive Sciences*, 25(1):37–54, January 2021.
- [4] Eloy Parra-Barrero, Sandhiya Vijayabaskaran, Eddie Seabrook, Laurenz Wiskott, and Sen Cheng. A map of spatial navigation for neuroscience. *Neuroscience & Biobehavioral Reviews*, 152:105200, September 2023.
- [5] Illeana Prieto, Dominic M. D. Tran, and Evan J. Livesey. Planning on Autopilot? Associative Contributions to Proactive Control. *Cognition*, 231:105321, February 2023.
- [6] Kinga Iglói, Christian F. Doeller, Alain Berthoz, Laure Rondi-Reig, and Neil Burgess. Lateralized human hippocampal activity predicts navigation based on sequence or place memory. *Proceedings of the National Academy of Sciences*, 107(32):14466–14471, August 2010.
- [7] Sarah C. Goodroe, Jon Starnes, and Thackery I. Brown. The Complex Nature of Hippocampal-Striatal Interactions in Spatial Navigation. *Frontiers in Human Neuroscience*, 12, June 2018.
- [8] Cheng Wang, Xiaojing Chen, and James J Knierim. Egocentric and allocentric representations of space in the rodent brain. *Current Opinion in Neurobiology*, 60:12–20, February 2020.
- [9] Lukas Kunz, Armin Brandt, Peter C. Reinacher, Bernhard P. Staresina, Eric T. Reifensstein, Christoph T. Weidemann, Nora A. Herweg, Ansh Patel, Melina Tsitsiklis, Richard Kempter, Michael J. Kahana, Andreas Schulze-Bonhage, and Joshua Jacobs. A neural code for egocentric spatial maps in the human medial temporal lobe. *Neuron*, 109(17):2781–2796.e10, September 2021.
- [10] Jason J. Moore, Jesse D. Cushman, Lavanya Acharya, Briana Popeney, and Mayank R. Mehta. Linking hippocampal multiplexed tuning, Hebbian plasticity and navigation. *Nature*, 599(7885):442–448, November 2021.

- [11] William H. Warren. Non-Euclidean navigation. *Journal of Experimental Biology*, 222(Suppl_1):jeb187971, February 2019.
- [12] Denis C. L. Lan, Laurence T. Hunt, and Christopher Summerfield. Goal-directed navigation in humans and deep reinforcement learning agents relies on an adaptive mix of vector-based and transition-based strategies. *PLOS Biology*, 23(7):e3003296, July 2025.
- [13] Stefano Recanatesi, Matthew Farrell, Guillaume Lajoie, Sophie Deneve, Mattia Rigotti, and Eric Shea-Brown. Predictive learning as a network mechanism for extracting low-dimensional latent space representations. *Nature Communications*, 12(1):1417, March 2021.
- [14] Fabian Kessler, Julia Frankenstein, and Constantin A. Rothkopf. Human navigation strategies and their errors result from dynamic interactions of spatial uncertainties. *Nature Communications*, 15(1):5677, July 2024.
- [15] Christoph Stöckl, Yukun Yang, and Wolfgang Maass. Local prediction-learning in high-dimensional spaces enables neural networks to plan. *Nature Communications*, 15(1):2344, March 2024.
- [16] Andrea Banino, Caswell Barry, Benigno Uria, Charles Blundell, Timothy Lillicrap, Piotr Mirowski, Alexander Pritzel, Martin J. Chadwick, Thomas Degris, Joseph Modayil, Greg Wayne, Hubert Soyer, Fabio Viola, Brian Zhang, Ross Goroshin, Neil Rabinowitz, Razvan Pascanu, Charlie Beattie, Stig Petersen, Amir Sadik, Stephen Gaffney, Helen King, Koray Kavukcuoglu, Demis Hassabis, Raia Hadsell, and Dharmashan Kumaran. Vector-based navigation using grid-like representations in artificial agents. *Nature*, 557(7705):429–433, May 2018.
- [17] Christopher J. Cueva and Xue-Xin Wei. Emergence of grid-like representations by training recurrent neural networks to perform spatial localization, March 2018.
- [18] T. S. Collett, B. A. Cartwright, and B. A. Smith. Landmark learning and visuo-spatial memories in gerbils. *Journal of Comparative Physiology A*, 158(6):835–851, November 1986.
- [19] A.S. Etienne. How does path integration interact with olfaction, vision, and the representation of space? In *The Neurobiology of Spatial Behaviour*, pages 48–66. Oxford University Press, November 2003.
- [20] Mathias Franzius, Henning Sprekeler, and Laurenz Wiskott. Slowness and Sparseness Lead to Place, Head-Direction, and Spatial-View Cells. *PLOS Computational Biology*, 3(8), 2007.
- [21] Isabelle T. Garzorz and Paul R. MacNeilage. Visual-Vestibular Conflict Detection Depends on Fixation. *Current Biology*, 27(18):2856–2861.e4, September 2017.
- [22] Edmund T. Rolls, Robert G. Robertson, and Pierre Georges-François. Spatial View Cells in the Primate Hippocampus. *European Journal of Neuroscience*, 9(8):1789–1794, 1997.
- [23] Arne D. Ekstrom, Michael J. Kahana, Jeremy B. Caplan, Tony A. Fields, Eve A. Isham, Ehren L. Newman, and Itzhak Fried. Cellular networks underlying human spatial navigation. *Nature*, 425(6954):184–188, September 2003.

- [24] Joshua Jacobs, Michael J. Kahana, Arne D. Ekstrom, Matthew V. Mollison, and Itzhak Fried. A sense of direction in human entorhinal cortex. *Proceedings of the National Academy of Sciences*, 107(14):6487–6492, April 2010.
- [25] Dun Mao, Eric Avila, Baptiste Caziot, Jean Laurens, J. David Dickman, and Dora E. Angelaki. Spatial modulation of hippocampal activity in freely moving macaques. *Neuron*, 109(21):3521–3534.e6, November 2021.
- [26] Diego B. Piza, Benjamin W. Corrigan, Roberto A. Gulli, Sonia Do Carmo, A. Claudio Cuello, Lyle Muller, and Julio Martinez-Trujillo. Primacy of vision shapes behavioral strategies and neural substrates of spatial navigation in marmoset hippocampus. *Nature Communications*, 15(1):4053, May 2024.
- [27] Zahra M. Aghajan, Lavanya Acharya, Jason J. Moore, Jesse D. Cushman, Cliff Vuong, and Mayank R. Mehta. Impaired spatial selectivity and intact phase precession in two-dimensional virtual reality. *Nature Neuroscience*, 18(1):121–128, January 2015.
- [28] Lavanya Acharya, Zahra M. Aghajan, Cliff Vuong, Jason J. Moore, and Mayank R. Mehta. Causal Influence of Visual Cues on Hippocampal Directional Selectivity. *Cell*, 164(1):197–207, January 2016.
- [29] Aman B. Saleem and Laura Busse. Interactions between rodent visual and spatial systems during navigation. *Nature Reviews Neuroscience*, 24(8):487–501, August 2023.
- [30] Ariane S. Etienne. Navigation of a Small Mammal by Dead Reckoning and Local Cues. *Current Directions in Psychological Science*, 1(2):48–52, April 1992.
- [31] Damian J. Wallace, David S. Greenberg, Juergen Sawinski, Stefanie Rulla, Giuseppe Notaro, and Jason N. D. Kerr. Rats maintain an overhead binocular field at the expense of constant fusion. *Nature*, 498(7452):65–69, June 2013.
- [32] Zohar Hagbi and David Eilam. On heights and plains: How rodents from different habitats cope with three-dimensional environments? *PLOS ONE*, 17(3):e0265176, March 2022.
- [33] Desirée Colombo, Silvia Serino, Cosimo Tuena, Elisa Pedrolì, Antonios Dakanalis, Pietro Cipresso, and Giuseppe Riva. Egocentric and allocentric spatial reference frames in aging: A systematic review. *Neuroscience & Biobehavioral Reviews*, 80:605–621, September 2017.
- [34] Merve Tansan, Kim V. Nguyen, and Nora S. Newcombe. Spatial Navigation in Childhood and Aging. *Annual Review of Developmental Psychology*, 4(Volume 4, 2022):253–272, December 2022.
- [35] Thomas Wolbers and Jan M. Wiener. Challenges for identifying the neural mechanisms that support spatial navigation: The impact of spatial scale. *Frontiers in Human Neuroscience*, 8, August 2014.
- [36] Howard Eichenbaum. The role of the hippocampus in navigation is memory. *Journal of Neurophysiology*, 117(4):1785–1796, April 2017.
- [37] Oliver M. Vikbladh, Michael R. Meager, John King, Karen Blackmon, Orrin Devinsky, Daphna Shohamy, Neil Burgess, and Nathaniel D. Daw. Hippocampal Contributions to Model-Based Planning and Spatial Memory. *Neuron*, 102(3):683–693.e4, May 2019.

- [38] Renaud Bastien and Pawel Romanczuk. A model of collective behavior based purely on vision. *Science Advances*, 6(6), February 2020.
- [39] Grace Lindsay. Convolutional Neural Networks as a Model of the Visual System: Past, Present, and Future. *Journal of Cognitive Neuroscience*, 33(10):2017–2031, October 2021.
- [40] Tim Salimans, Jonathan Ho, Xi Chen, Szymon Sidor, and Ilya Sutskever. Evolution Strategies as a Scalable Alternative to Reinforcement Learning, September 2017.
- [41] Amjad Yousef Majid, Serge Saaybi, Tomas van Rietbergen, Vincent Francois-Lavet, R. Venkatesha Prasad, and Chris Verhoeven. Deep Reinforcement Learning Versus Evolution Strategies: A Comparative Survey, September 2021.
- [42] Dian Anggraini, Stefan Glasauer, and Klaus Wunderlich. Neural signatures of reinforcement learning correlate with strategy adoption during spatial navigation. *Scientific Reports*, 8(1):10110, July 2018.
- [43] Edgar Bermudez-Contreras, Benjamin J. Clark, and Aaron Wilber. The Neuroscience of Spatial Navigation and the Relationship to Artificial Intelligence. *Frontiers in Computational Neuroscience*, 14, July 2020.
- [44] Sandhiya Vijayabaskaran and Sen Cheng. Navigation task and action space drive the emergence of egocentric and allocentric spatial representations. *PLOS Computational Biology*, 18(10):e1010320, October 2022.
- [45] Ayelet Sarel, Arseny Finkelstein, Liora Las, and Nachum Ulanovsky. Vectorial representation of spatial goals in the hippocampus of bats. *Science*, 355(6321):176–180, January 2017.
- [46] Roger A. Hart and Gary T. Moore. The Development of Spatial Cognition: A Review. In *Image & Environment: Cognitive Mapping and Spatial Behavior*, pages 246–288. AldineTransaction, New Brunswick, NJ, US, 1973.
- [47] Alexander W. Siegel and Sheldon H. White. The Development of Spatial Representations of Large-Scale Environments. In Hayne W. Reese, editor, *Advances in Child Development and Behavior*, volume 10, pages 9–55. JAI, January 1975.
- [48] Steven A. Marchette, Arnold Bakker, and Amy L. Shelton. Cognitive Mappers to Creatures of Habit: Differential Engagement of Place and Response Learning Mechanisms Predicts Human Navigational Behavior. *Journal of Neuroscience*, 31(43):15264–15268, October 2011.
- [49] Amy L. Shelton, Steven A. Marchette, and Andrew J. Furman. Chapter Six - A Mechanistic Approach to Individual Differences in Spatial Learning, Memory, and Navigation. In Brian H. Ross, editor, *Psychology of Learning and Motivation*, volume 59, pages 223–259. Academic Press, January 2013.
- [50] Steven M. Weisberg and Nora S. Newcombe. Cognitive Maps: Some People Make Them, Some People Struggle. *Current Directions in Psychological Science*, 27(4):220–226, August 2018.
- [51] Rüdiger Wehner and Sibylle Wehner. Parallel evolution of thermophilia: Daily and seasonal foraging patterns of heat-adapted desert ants: *Cataglyphis* and *Ocymyrmex* species. *Physiological Entomology*, 36(3):271–281, 2011.

-
- [52] Benedicte M. Babayan, Aurélie Watilliaux, Guillaume Viejo, Anne-Lise Paradis, Benoît Girard, and Laure Rondi-Reig. A hippocampo-cerebellar centred network for the learning and execution of sequence-based navigation. *Scientific Reports*, 7(1):17812, December 2017.
 - [53] Hugo J. Spiers, Antoine Coutrot, and Michael Hornberger. How the environment shapes our ability to navigate. *Clinical and Translational Medicine*, 12(6):e928, June 2022.
 - [54] Nathaniel D. Daw, Yael Niv, and Peter Dayan. Uncertainty-based competition between prefrontal and dorsolateral striatal systems for behavioral control. *Nature Neuroscience*, 8(12):1704–1711, December 2005.
 - [55] Wendy Wood and Dennis R  nger. Psychology of Habit. *Annual Review of Psychology*, 67(Volume 67, 2016):289–314, January 2016.
 - [56] Mehdi Khamassi and Mark D. Humphries. Integrating cortico-limbic-basal ganglia architectures for learning model-based and model-free navigation strategies. *Frontiers in Behavioral Neuroscience*, 6, November 2012.
 - [57] Nora A. Herweg and Michael J. Kahana. Spatial Representations in the Human Brain. *Frontiers in Human Neuroscience*, 12, July 2018.
 - [58] Anusha Nagabandi, Gregory Kahn, Ronald S. Fearing, and Sergey Levine. Neural Network Dynamics for Model-Based Deep Reinforcement Learning with Model-Free Fine-Tuning. In *2018 IEEE International Conference on Robotics and Automation (ICRA)*, pages 7559–7566, May 2018.
 - [59] Dongjae Kim, Geon Yeong Park, John P. O’Doherty, and Sang Wan Lee. Task complexity interacts with state-space uncertainty in the arbitration between model-based and model-free learning. *Nature Communications*, 10(1):5738, December 2019.
 - [60] Christian F. Doeller, John A. King, and Neil Burgess. Parallel striatal and hippocampal systems for landmarks and boundaries in spatial memory. *Proceedings of the National Academy of Sciences*, 105(15):5915–5920, April 2008.
 - [61] Deirdre R. Harvey, Anne-Marie T. McGauran, Jonathan Murphy, Lauren Burns, Eoghan McMonagle, and Sean Commins. Emergence of an egocentric cue guiding and allocentric inferring strategy that mirrors hippocampal brain-derived neurotrophic factor (BDNF) expression in the Morris water maze. *Neurobiology of Learning and Memory*, 89(4):462–479, May 2008.
 - [62] Cheng Wang, Xiaojing Chen, Heekyung Lee, Sachin S. Deshmukh, D. Yoganarasimha, Francesco Savelli, and James J. Knierim. Egocentric coding of external items in the lateral entorhinal cortex | Science. *Science Advances*, 362, 2018.
 - [63] James P. Rice, Douglas G. Wallace, and Derek A. Hamilton. Lesions of the hippocampus or dorsolateral striatum disrupt distinct aspects of spatial navigation strategies based on proximal and distal information in a cued variant of the Morris water task. *Behavioural Brain Research*, 289:105–117, August 2015.

- [64] Akinori Higaki, Masaki Mogi, Jun Iwanami, Li-Juan Min, Hui-Yu Bai, Bao-Shuai Shan, Harumi Kan-no, Shuntaro Ikeda, Jitsuo Higaki, and Masatsugu Horiuchi. Recognition of early stage thigmotaxis in Morris water maze test with convolutional neural network. *PLOS ONE*, 13(5):e0197003, May 2018.
- [65] Nadine Curdt, Franziska W. Schmitt, Caroline Bouter, Trendelina Iseni, Hanna C. Weile, Berfin Altunok, Nicola Beindorff, Thomas A. Bayer, Matthew B. Cooke, and Yvonne Bouter. Search strategy analysis of Tg4-42 Alzheimer Mice in the Morris Water Maze reveals early spatial navigation deficits. *Scientific Reports*, 12(1):5451, March 2022.
- [66] Stephen D. Auger, Sinéad L. Mullally, and Eleanor A. Maguire. Retrosplenial Cortex Codes for Permanent Landmarks. *PLOS ONE*, 7(8):e43620, August 2012.
- [67] Michael F. Bonner and Russell A. Epstein. Coding of navigational affordances in the human visual system. *Proceedings of the National Academy of Sciences*, 114(18):4793–4798, May 2017.
- [68] Aman B. Saleem, E. Mika Diamanti, Julien Fournier, Kenneth D. Harris, and Matteo Carandini. Coherent encoding of subjective spatial position in visual cortex and hippocampus. *Nature*, 562(7725):124–127, October 2018.
- [69] Sven Krausse, Emre Neftci, and Friedrich T Sommer. The head-direction system shows systematic parallax error. In *CCN 2025*, August 2025.
- [70] Pierre-Yves Jacob, Giulio Casali, Laure Spieser, Hector Page, Dorothy Overington, and Kate Jeffery. An independent, landmark-dominated head-direction signal in dysgranular retrosplenial cortex. *Nature Neuroscience*, 20(2):173–175, February 2017.
- [71] Olga Kornienko, Patrick Latuske, Mathis Bessler, Laura Kohler, and Kevin Allen. Non-rhythmic head-direction cells in the parahippocampal region are not constrained by attractor network dynamics. *eLife*, 7:e35949, September 2018.
- [72] Dominique Siegenthaler, Henry Denny, Sofía Skromne Carrasco, Johanna Luise Mayer, Daniel Levenstein, Adrien Peyrache, Stuart Trenholm, and Émilie Macé. Visual objects refine head direction coding. *Science*, 389(6765):eadu9828, September 2025.
- [73] Jake Ormond and John O’Keefe. Hippocampal place cells have goal-oriented vector fields during navigation. *Nature*, 607(7920):741–746, July 2022.
- [74] Andrew S. Alexander, Lucas C. Carstensen, James R. Hinman, Florian Raudies, G. William Chapman, and Michael E. Hasselmo. Egocentric boundary vector tuning of the retrosplenial cortex | Science Advances. *Science Advances*, 6(8), 2020.
- [75] Matej Hoffmann and Rolf Pfeifer. Robots as powerful allies for the study of embodied cognition from the bottom up. In Albert Newen, Leon De Bruin, and Shaun Gallagher, editors, *The Oxford Handbook of 4E Cognition*, page 0. Oxford University Press, September 2018.

- [76] Jan Degenaar and J. Kevin O'Regan. Sensorimotor Theory and Enactivism. *Topoi*, 36(3):393–407, September 2017.
- [77] Matthew D. Egbert and Xabier E. Barandiaran. Using enactive robotics to think outside of the problem-solving box: How sensorimotor contingencies constrain the forms of emergent autonomous habits. *Frontiers in Neurobotics*, 16, December 2022.
- [78] Ipshita Zutshi, Athina Apostolelli, Wannan Yang, Zheyang Zheng, Tora Dohi, Edoardo Balzani, Alex H Williams, Cristina Savin, and Buzsaki. Hippocampal neuronal activity is aligned with action plans. *Nature*, 639:153–161, January 25.
- [79] Steven M. Weisberg, Victor R. Schinazi, Nora S. Newcombe, Thomas F. Shipley, and Russell A. Epstein. Variations in cognitive maps: Understanding individual differences in navigation. *Journal of Experimental Psychology: Learning, Memory, and Cognition*, 40(3):669–682, 2014.
- [80] Matthew B. Cooke, Timothy P. O'Leary, Phelan Harris, Ricky Ma, Richard E. Brown, and Jason S. Snyder. Pathfinder: Open source software for analyzing spatial navigation search strategies. *F1000Research*, 8:1521, June 2020.
- [81] Eliud Enrique Villarreal-Silva, Alejandro Rafael González-Navarro, Rodolfo Amador Salazar-Ybarra, Oscar Quiroga-García, Miguel Angel de Jesús Cruz-Elizondo, Aracely García-García, Humberto Rodríguez-Rocha, Jesús Alberto Morales-Gómez, Alejandro Quiroga-Garza, Rodrigo Enrique Elizondo-Omaña, Ángel Raymundo Martínez-Ponce de León, and Santos Guzmán-López. Aged rats learn Morris Water maze using non-spatial search strategies evidenced by a parameter-based algorithm. *Translational Neuroscience*, 13(1):134–144, January 2022.
- [82] Alessandro Graziano, Laura Petrosini, and Alessandro Bartoletti. Automatic recognition of explorative strategies in the Morris water maze. *Journal of Neuroscience Methods*, 130(1):33–44, November 2003.
- [83] Luis Alvarez, Benjamin M. Friedrich, Gerhard Gompfer, and U. Benjamin Kaupp. The computational sperm cell. *Trends in Cell Biology*, 24(3):198–207, March 2014.
- [84] Julian Rode, Maja Novak, and Benjamin M. Friedrich. Information Theory of Chemotactic Agents Using Both Spatial and Temporal Gradient Sensing. *PRX Life*, 2(2):023012, June 2024.
- [85] Vivek H. Sridhar, Liang Li, Dan Gorbonos, Máté Nagy, Bianca R. Schell, Timothy Sorochkin, Nir S. Gov, and Iain D. Couzin. The geometry of decision-making in individuals and collectives. *Proceedings of the National Academy of Sciences*, 118(50):e2102157118, December 2021.
- [86] Dan Gorbonos, Nir S. Gov, and Iain D. Couzin. Geometrical Structure of Bifurcations during Spatial Decision-Making. *PRX Life*, 2(1):013008, February 2024.
- [87] Antoine Wystrach, Alex Dewar, Andrew Philippides, and Paul Graham. How do field of view and resolution affect the information content of panoramic scenes for visual navigation? A computational investigation. *Journal of Comparative Physiology A*, 202(2):87–95, February 2016.

-
- [88] Jochen Zeil. Visual navigation: Properties, acquisition and use of views. *Journal of Comparative Physiology A*, 209(4):499–514, July 2023.
 - [89] A. F. Sanders. Some Aspects of the Selective Process in the Functional Visual Field. *Ergonomics*, 13(1):101–117, January 1970.
 - [90] György Buzsáki and Kenji Mizuseki. The log-dynamic brain: How skewed distributions affect network operations. *Nature Reviews Neuroscience*, 15(4):264–278, April 2014.
 - [91] Edgar Chan, Oliver Baumann, Mark Bellgrove, and Jason Mattingley. From Objects to Landmarks: The Function of Visual Location Information in Spatial Navigation. *Frontiers in Psychology*, 3, 2012.
 - [92] Ranxiao Frances Wang and Elizabeth S. Spelke. Human spatial representation: Insights from animals. *Trends in Cognitive Sciences*, 6(9):376–382, September 2002.
 - [93] Sang Ah Lee and Elizabeth S. Spelke. Two systems of spatial representation underlying navigation. *Experimental Brain Research*, 206(2):179–188, October 2010.
 - [94] Christian F. Doeller and Neil Burgess. Distinct error-correcting and incidental learning of location relative to landmarks and boundaries. *Proceedings of the National Academy of Sciences*, 105(15):5909–5914, April 2008.
 - [95] Zhuang Liu, Hanzi Mao, Chao-Yuan Wu, Christoph Feichtenhofer, Trevor Darrell, and Saining Xie. A ConvNet for the 2020s. In *Proceedings of the IEEE/CVF Conference on Computer Vision and Pattern Recognition*, pages 11976–11986, 2022.
 - [96] Sanghyun Woo, Shoubhik Debnath, Ronghang Hu, Xinlei Chen, Zhuang Liu, In So Kweon, and Saining Xie. ConvNeXt V2: Co-Designing and Scaling ConvNets With Masked Autoencoders. In *Proceedings of the IEEE/CVF Conference on Computer Vision and Pattern Recognition*, pages 16133–16142, 2023.
 - [97] Salman Khan, Muzammal Naseer, Munawar Hayat, Syed Waqas Zamir, Fahad Shahbaz Khan, and Mubarak Shah. Transformers in Vision: A Survey. *ACM Computing Surveys*, 54(10s):200:1–200:41, September 2022.
 - [98] Chunyuan Li, Heerad Farkhoor, Rosanne Liu, and Jason Yosinski. Measuring the Intrinsic Dimension of Objective Landscapes, April 2018.
 - [99] Frank Sehnke, Christian Osendorfer, Thomas Rückstieß, Alex Graves, Jan Peters, and Jürgen Schmidhuber. Parameter-exploring policy gradients. *Neural Networks*, 23(4):551–559, May 2010.
 - [100] Nihat Engin Toklu, Paweł Liskowski, and Rupesh Kumar Srivastava. ClipUp: A Simple and Powerful Optimizer for Distribution-Based Policy Evolution. In Thomas Bäck, Mike Preuss, André Deutz, Hao Wang, Carola Doerr, Michael Emmerich, and Heike Trautmann, editors, *Parallel Problem Solving from Nature – PPSN XVI*, Lecture Notes in Computer Science, pages 515–527, Cham, 2020. Springer International Publishing.
 - [101] David Ha. A Visual Guide to Evolution Strategies, October 2017.
 - [102] Leah Armon, S. Roy Caplan, Michael Eisenbach, and Benjamin M. Friedrich. Testing Human Sperm Chemotaxis: How to Detect Biased Motion in Population Assays. *PLOS ONE*, 7(3):e32909, March 2012.

-
- [103] Claude Elwood Shannon and Warren Weaver. *The Mathematical Theory of Communication, by CE Shannon (and Recent Contributions to the Mathematical Theory of Communication)*. University of illinois Press, Champaign, IL, USA, 1949.
- [104] K. R. Pilkiewicz, B. H. Lemasson, M. A. Rowland, A. Hein, J. Sun, A. Berdahl, M. L. Mayo, J. Moehlis, M. Porfiri, E. Fernández-Juricic, S. Garnier, E. M. Bollt, J. M. Carlson, M. R. Tarampi, K. L. Macuga, L. Rossi, and C.-C. Shen. Decoding collective communications using information theory tools. *Journal of The Royal Society Interface*, 17(164):20190563, March 2020.

6 Supporting information

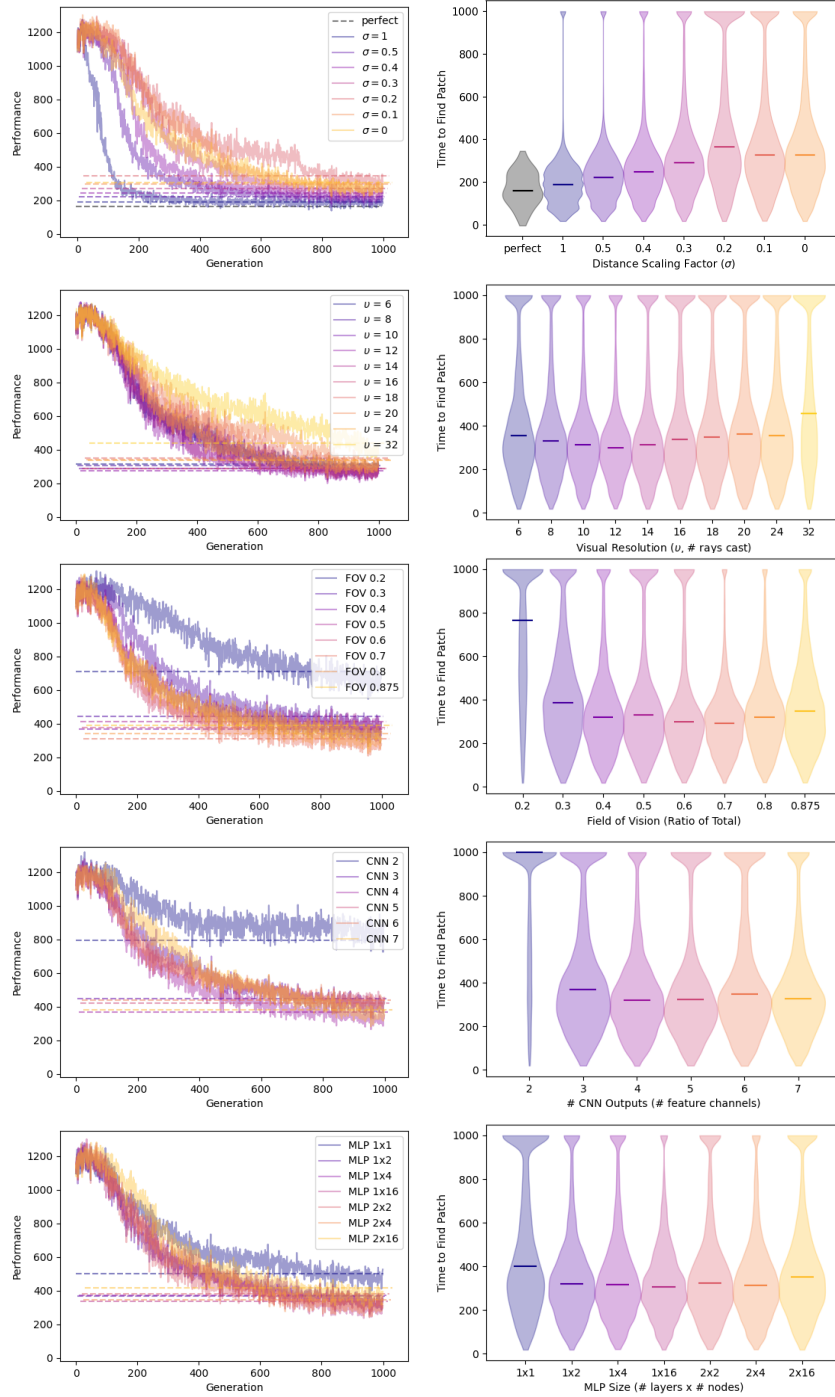


Fig S1: Evolutionary performance with differing parameters. Left: median performance of 40 training runs, dashed lines indicate median of validation tests. Right: validation test distribution (remaining distance to patch not included), lines indicate median, same color as legend in left plot. Runs used in top figure reflect data used in main text (perfect: theoretical lower bound). Unless otherwise noted, parameters are as follows: Distance scaling factor (σ): 0; Visual resolution (ν): 8; Field of vision: 0.4; CNN output size: 4; Multilayer perceptron (MLP) size: 1x2.

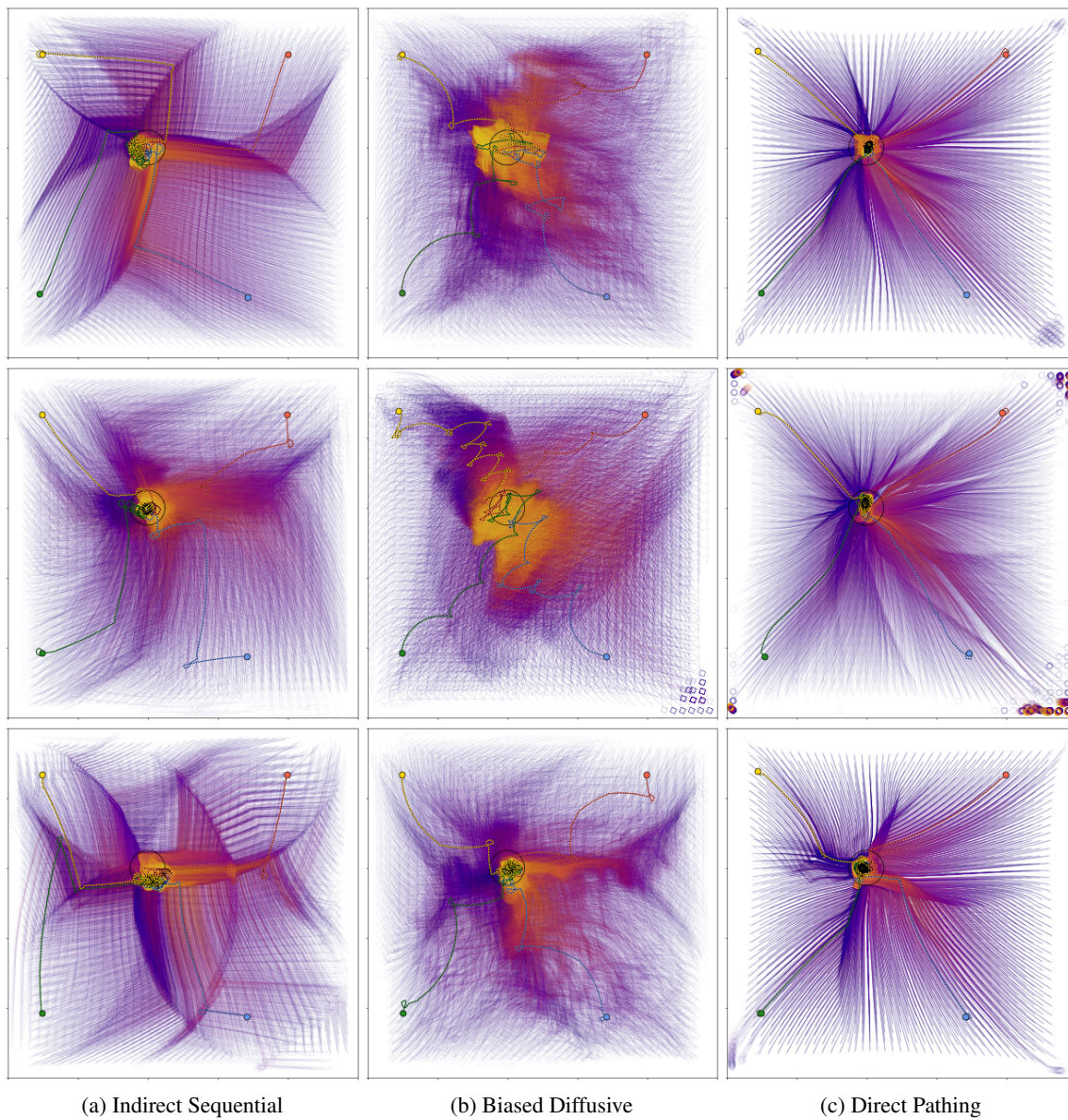


Fig S2: Extended figure from Fig 2 top row trajectories. Top/middle rows: $v = 8$. Bottom row: $v = 16$. See S3 Fig for corresponding correlations.

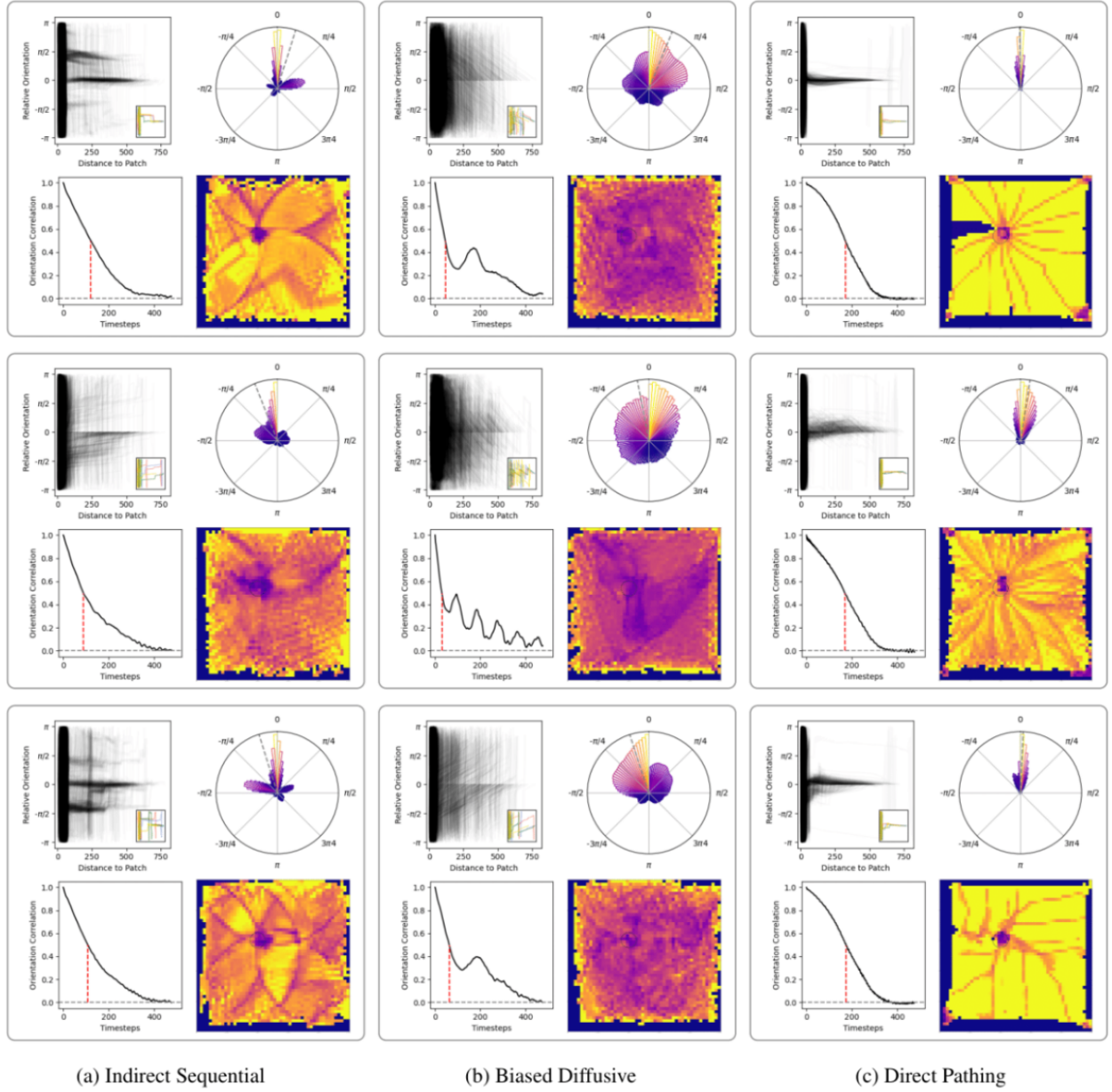


Fig S3: **Extended figure from Fig 2 bottom row correlations.** Top/middle rows: $\nu = 8$. Bottom row: $\nu = 16$. See S2 Fig for corresponding trajectories.

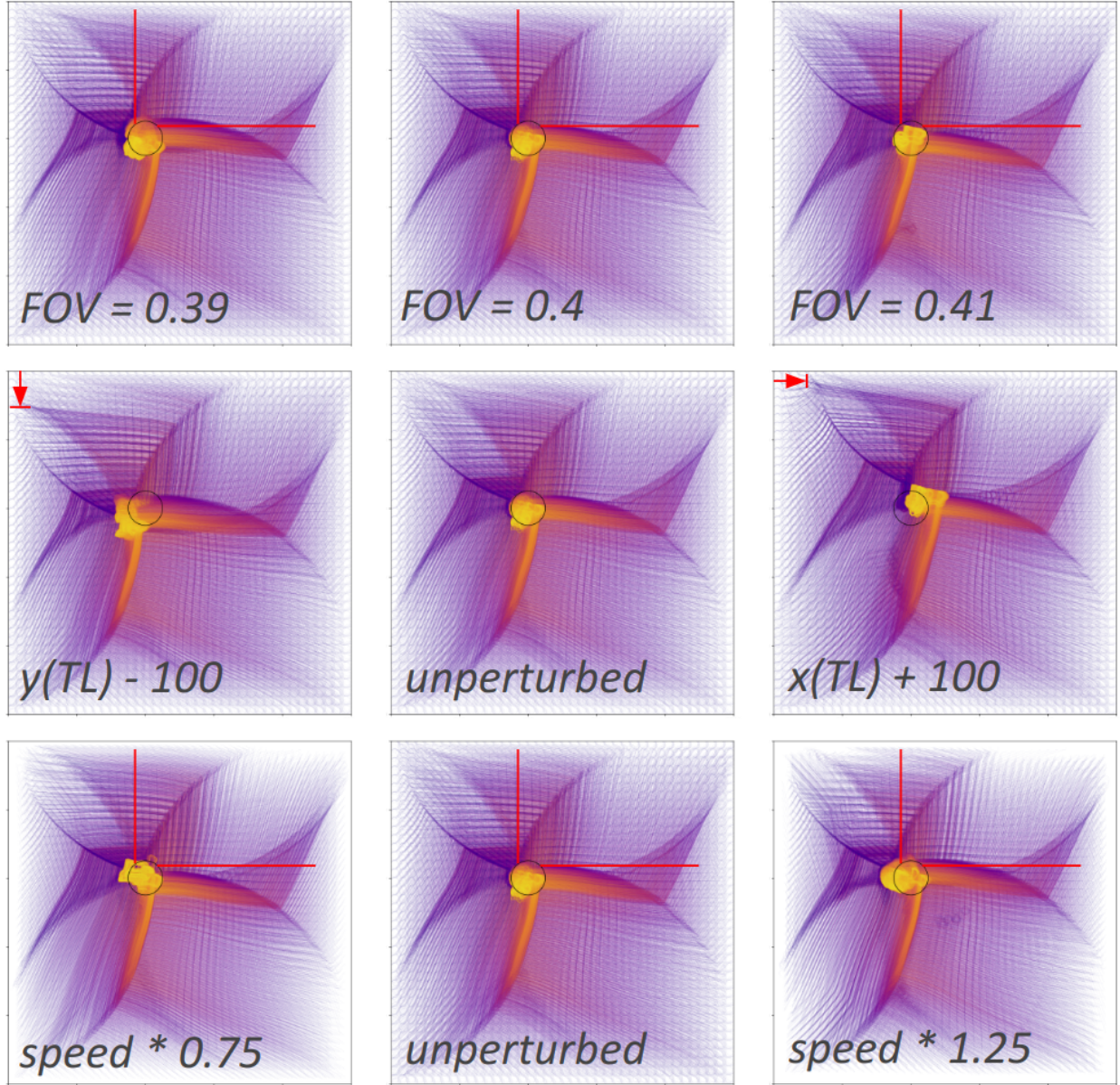


Fig S4: **Perturbations to a trained agent (perception, environment, action).** Top row: perturbation of field of vision. Middle row: perturbation of NW (top left) corner. Bottom row: perturbation of agent speed. Middle column: unperturbed agent. Red lines: visual guides.

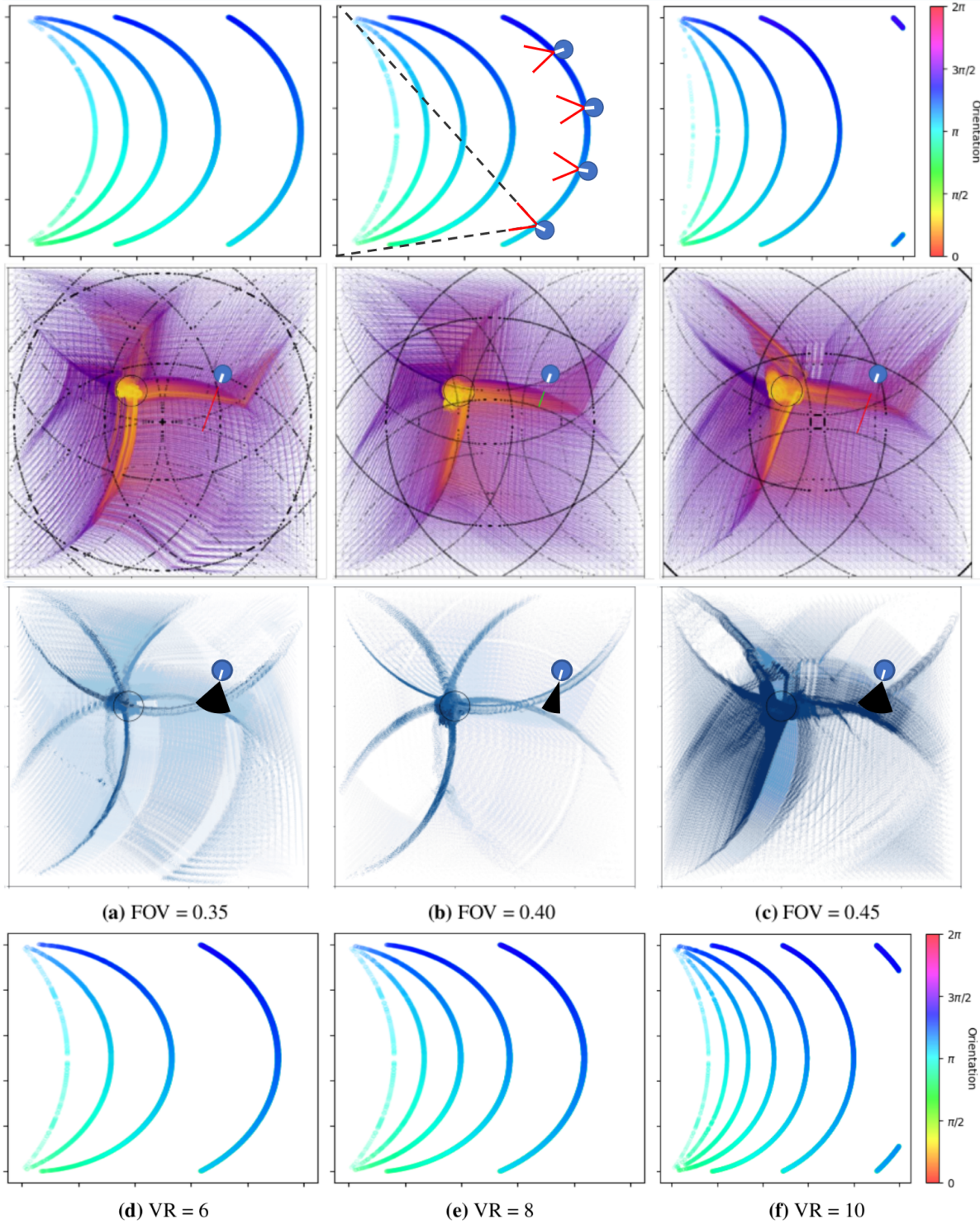


Fig S5: **Dual corner raycast as elliptical decision manifold.** 1st row: ideal locations for double detection of the top-left/bottom-left corners, for differing field of vision parameters, where the agents in (b) illustrate example agent positions and orientations along one of the available elliptical arcs. As the agent is rotated, visual observation remains the same, allowing a consistent action to be tied across the manifold. 2nd row: trajectory maps with points plotted for simultaneous dual corner raycasts. 3rd row: absolute value of turning speed, normalized between 0 and 90 degrees per timestep. 4th row: same as 1st but for differing visual resolutions.

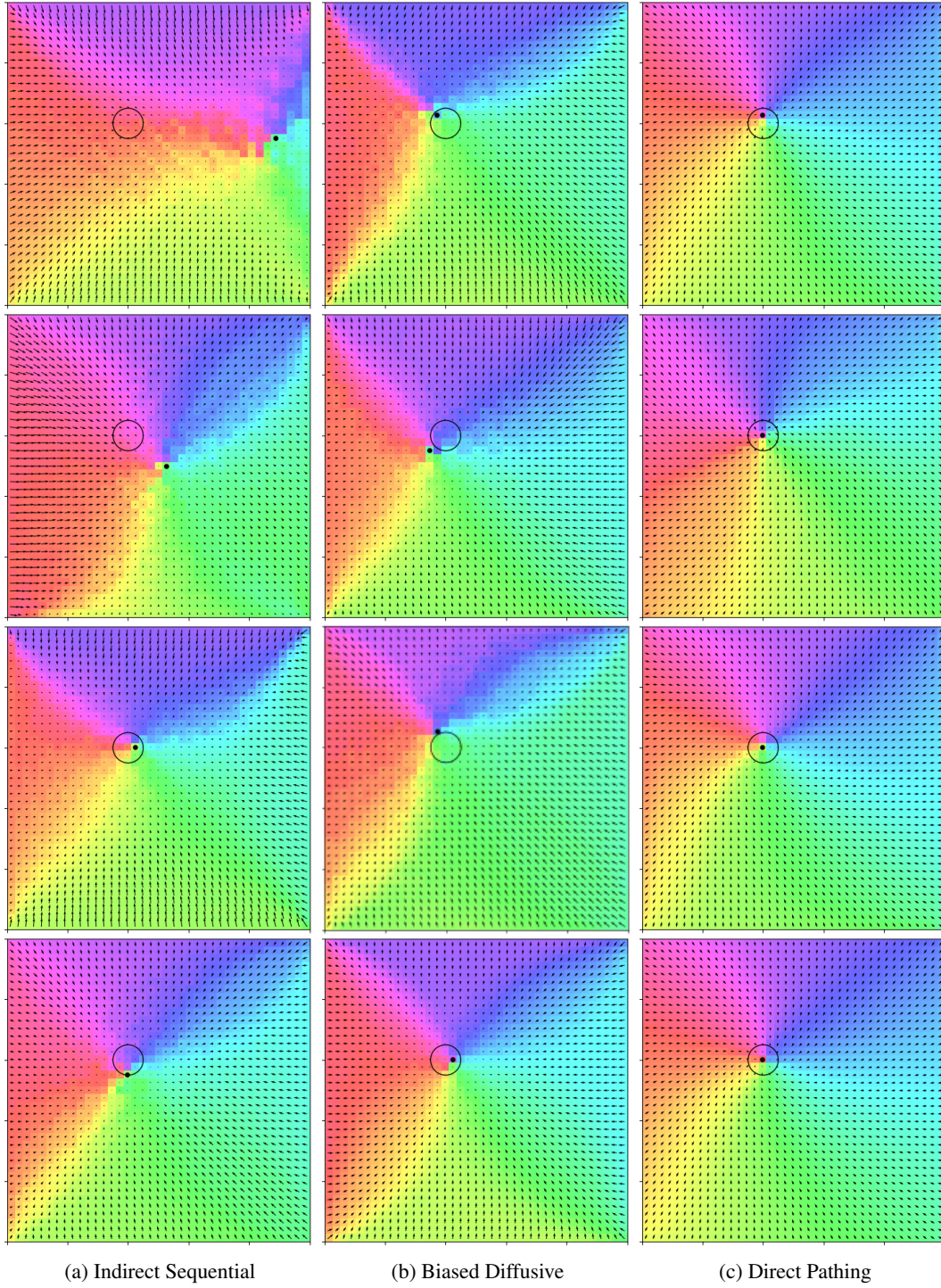


Fig S6: **Mean action vector fields.** Mean vectors are computed and plotted for agent action outputs at 64 unique orientations for each grid location. Mean vector orientation are plotted with colors following the colorbar in Fig S5. Agents used mirror those in Fig 2 (top row) & S2 Fig (bottom three). Black points signify global minima in mean vector magnitude.

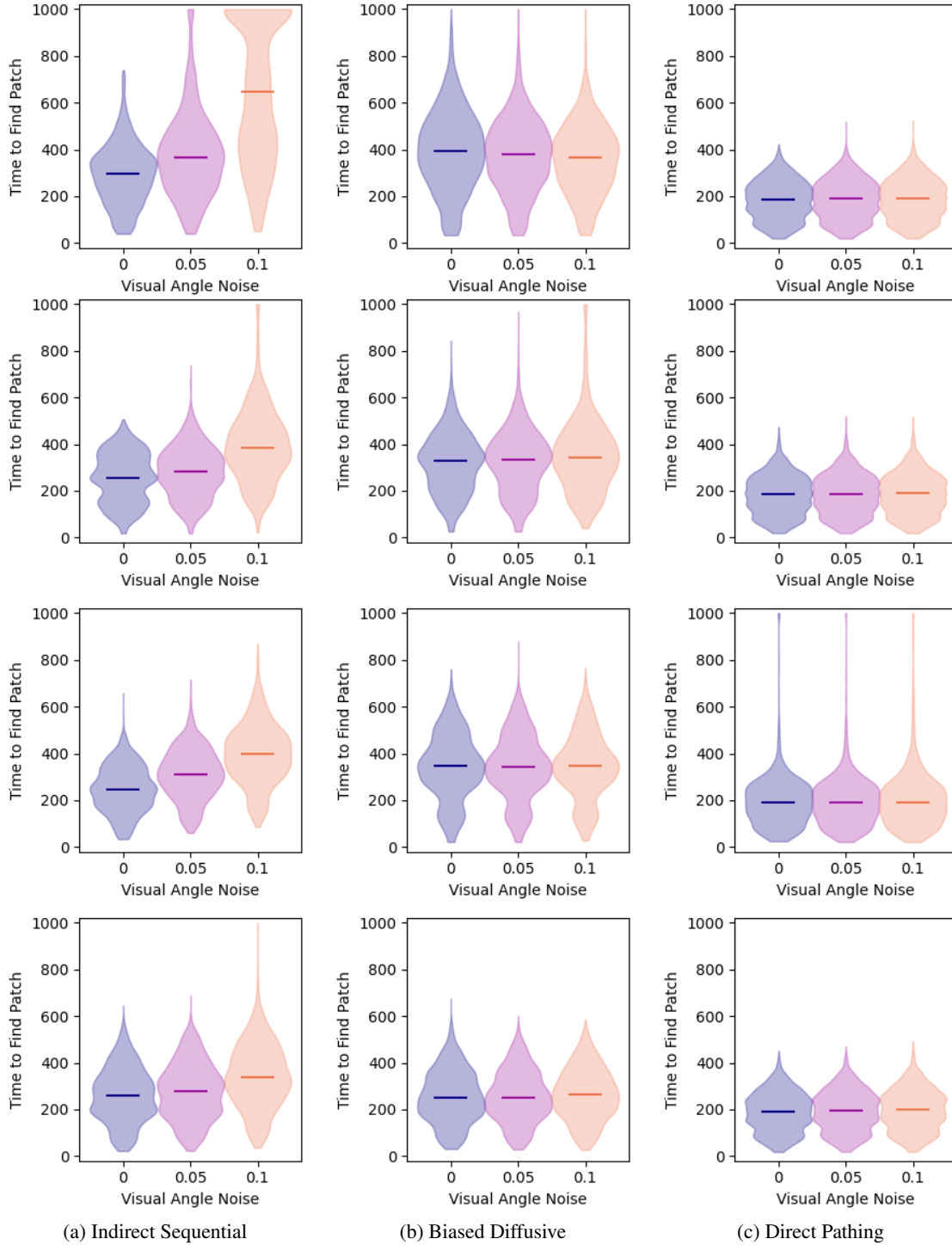


Fig S7: **Effect of noise to the visual angle.** Visual angle, as the median of an agent FOV, is perturbed by Gaussian noise with the two standard deviation of 0.05 and 0.1 radians. Same set of initializations/networks as in Fig 2 (top row) & S2 Fig (bottom three).

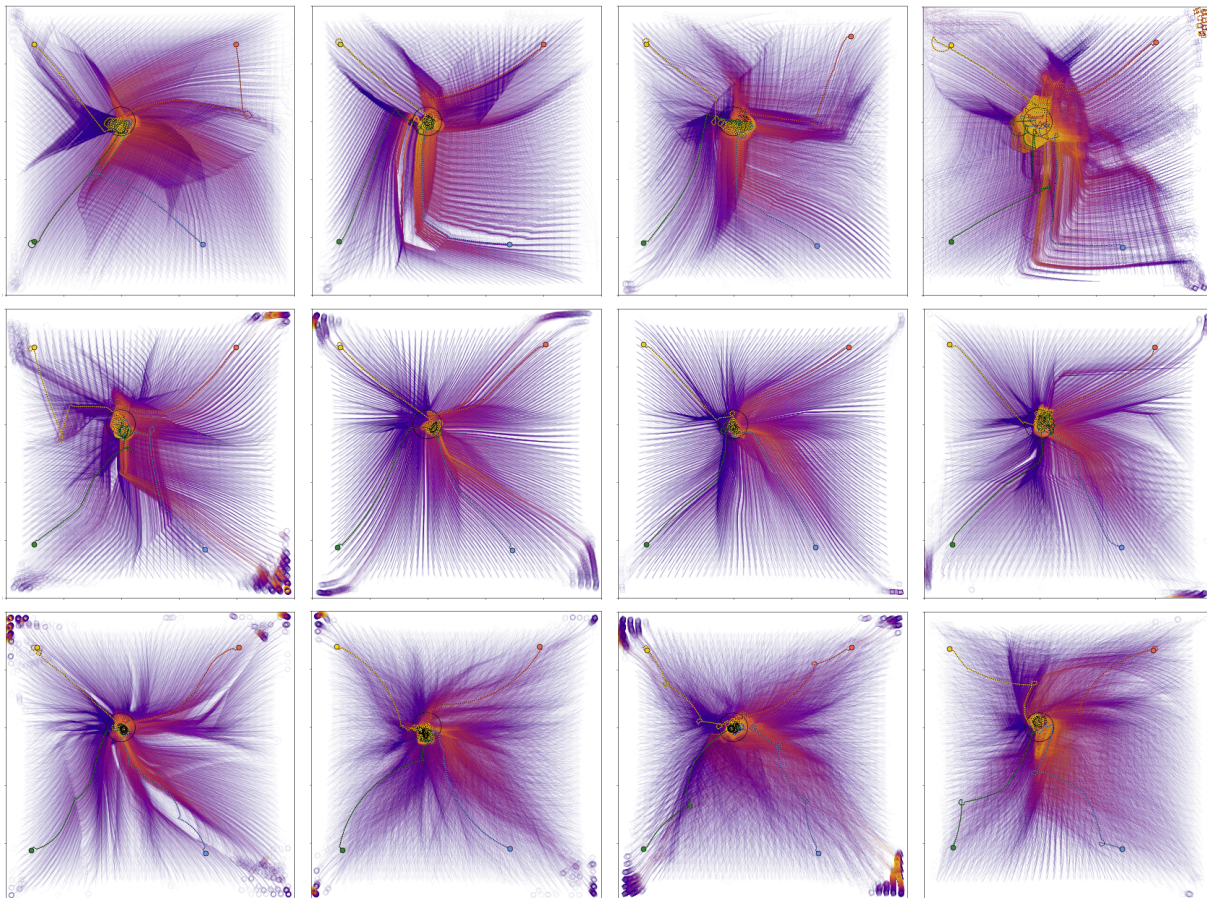


Fig S8: **A collection of trajectory plots representing behavioral hybridization possible.** σ damped to 0.5, midway between Fig 2 A/B & C, at visual resolution 8, arranged as a double continuum of classes: from indirect sequential to direct pathing to biased diffusion.

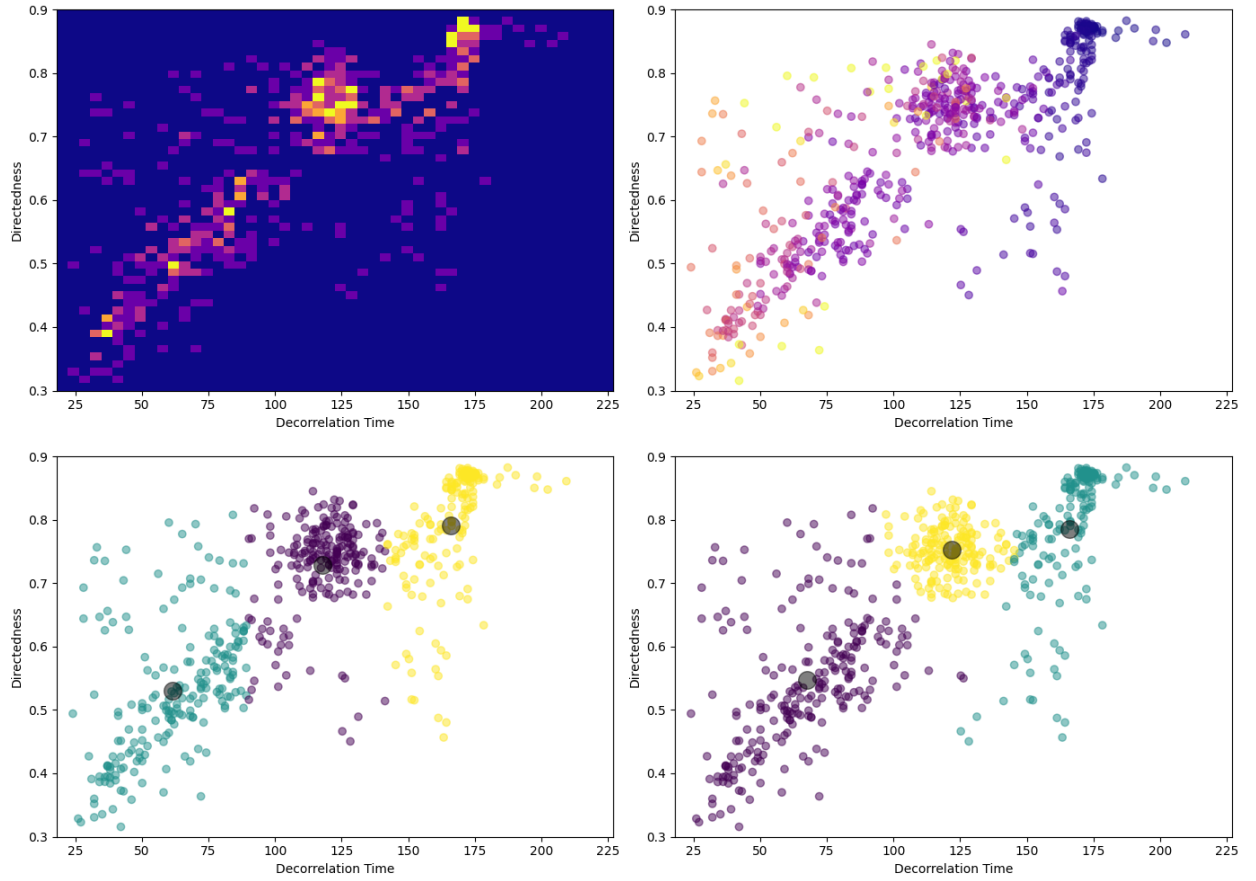


Fig S9: **Extended data for Fig 4.** Top left: density-based heatmap, maximum in yellow normalized at 5. Top right: relative fitnesses (blue: maximum, yellow: minimum). Bottom row: unsupervised clustering (left: K-Means, right: gaussian mixture), cluster centers plotted as larger circles.

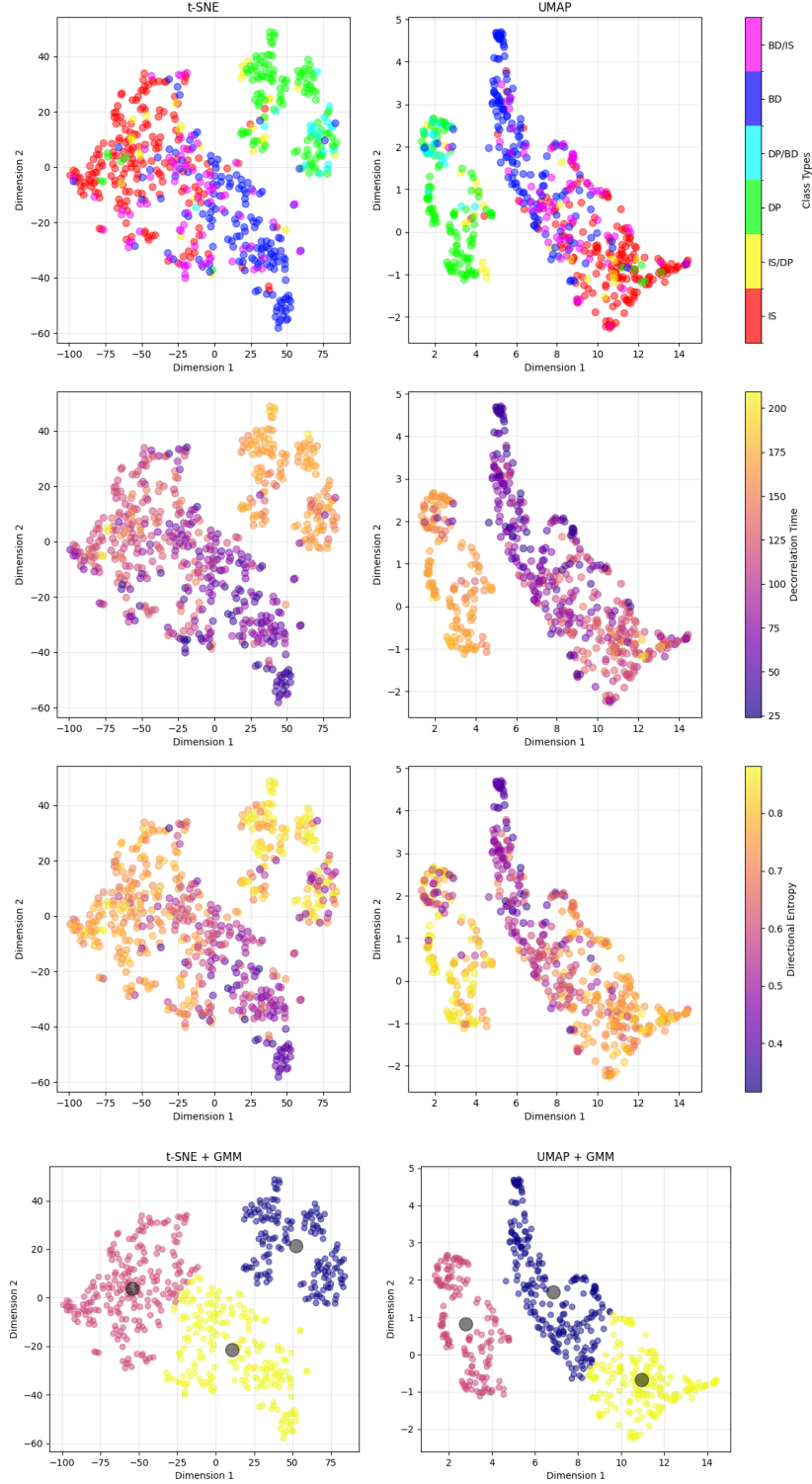


Fig S10: Classification via dimensionality reduction: t-SNE (left) & UMAP (right). Sets of actions associated with visual observations from 132 positions and orientations in the environment for the trained agents of each evolutionary run were passed through the two dimensionality reduction procedures. Results are plotted according to: 1st row: classification labels from the metric-based procedure as illustrated in Fig 4, 2nd row: decorrelation time, 3rd row: directional entropy 4th row: Gaussian mixture models were fit to the results, redrawing similar class boundaries.